

This discussion paper is/has been under review for the journal Earth System Science Data (ESSD). Please refer to the corresponding final paper in ESSD if available.

# CoastColour Round Robin datasets: a database to evaluate the performance of algorithms for the retrieval of water quality parameters in coastal waters

B. Nechad<sup>1</sup>, K. Ruddick<sup>1</sup>, T. Schroeder<sup>2</sup>, K. Oubelkheir<sup>2</sup>, D. Blondeau-Patissier<sup>3</sup>,  
N. Cherukuru<sup>2</sup>, V. Brando<sup>2</sup>, A. Dekker<sup>2</sup>, L. Clementson<sup>2</sup>, A. C. Banks<sup>4,19</sup>,  
S. Maritorenà<sup>5</sup>, J. Werdell<sup>6</sup>, C. Sá<sup>7</sup>, V. Brotas<sup>7</sup>, I. Caballero de Frutos<sup>8</sup>,  
Y.-H. Ahn<sup>9</sup>, S. Salama<sup>10</sup>, G. Tilstone<sup>11</sup>, V. Martinez-Vicente<sup>11</sup>, D. Foley<sup>12</sup>,  
M. McKibben<sup>13</sup>, J. Nahorniak<sup>13</sup>, T. Peterson<sup>14</sup>, A. Siliò-Calzada<sup>15</sup>, R. Röttgers<sup>16</sup>,  
Z. Lee<sup>17</sup>, M. Peters<sup>18</sup>, and C. Brockmann<sup>18</sup>

<sup>1</sup>Operational Directorate Natural Environment, Royal Belgian Institute for Natural Sciences (RBINS/ODNE), 100 Gulledele Brussels, 1200, Belgium

<sup>2</sup>Commonwealth Scientific and Industrial Research Organisation (CSIRO), Australia

<sup>3</sup>Charles Darwin University, 0815 Darwin, Australia

<sup>4</sup>Hellenic Centre for Marine Research (HCMR), Institute of Oceanography, P.O. Box 2214, Heraklion 71003, Crete, Greece

## CoastColour Round Robin datasets

B. Nechad et al.

Title Page

Abstract

Instruments

Data Provenance & Structure

Tables

Figures

◀

▶

◀

▶

Back

Close

Full Screen / Esc

Printer-friendly Version

Interactive Discussion



<sup>5</sup>Earth Research Institute (ERA), University of California, Santa Barbara, CA 93106-3060, USA

<sup>6</sup>NASA Goddard Space Flight Center, Greenbelt, Maryland 20771, USA

<sup>7</sup>Marine and Environmental Sciences Centre (MARE), Faculdade de Ciências da Universidade de Lisboa, Campo Grande, 1749-016 Lisbon, Portugal

<sup>8</sup>Institute of Marine Sciences of Andalusia (ICMAN-CSIC) Puerto Real-Cádiz, 11519, Spain

<sup>9</sup>Korea Ocean Research & Development Institute (KORDI) Ansan, P.O. Box 29, 425-600 Korea

<sup>10</sup>Faculty of Geo-information Science and Earth Observation (ITC) Hengelosestraat 99, 7514 AE Enschede, the Netherlands

<sup>11</sup>Plymouth Marine Laboratory, Prospect Place, The Hoe, Plymouth PL1 3DH, UK

<sup>12</sup>National Oceanic and Atmospheric Administration (NOAA), 1401 Constitution Avenue, NW, Washington DC 20230, USA

<sup>13</sup>College of Earth, Ocean and Atmospheric Sciences (CEOAS), Oregon State University, Corvallis, OR, USA

<sup>14</sup>Oregon Health and Science University, USA

<sup>15</sup>Environmental Hydraulics Institute of the University of Cantabria, Spain

<sup>16</sup>Institute of Coastal Research, Helmholtz-Zentrum Geesthacht, Centre Materials and Coastal Research, Max-Planck-Str.1, 21502 Geesthacht, Germany

<sup>17</sup>Centre for Materials and Coastal, University of Massachusetts, Boston, USA

<sup>18</sup>Brockmann Consult, Max-Planck-Str. 2, 21502 Geesthacht, Germany

<sup>19</sup>European Commission – Joint Research Centre (JRC), Institute for Environment and Sustainability, Via Enrico Fermi 2749, Ispra (Va) 21027, Italy

Received: 27 January 2015 – Accepted: 3 February 2015 – Published: 25 February 2015

Correspondence to: B. Nechad (b.nechad@mumm.ac.be)

Published by Copernicus Publications.

CoastColour Round Robin datasets

B. Nechad et al.

Title Page

Abstract

Instruments

Data Provenance & Structure

Tables

Figures

◀

▶

◀

▶

Back

Close

Full Screen / Esc

Printer-friendly Version

Interactive Discussion



## Abstract

The use of in situ measurements is essential in the validation and evaluation of the algorithms that provide coastal water quality data products from ocean colour satellite remote sensing. Over the past decade, various types of ocean colour algorithms have been developed to deal with the optical complexity of coastal waters. Yet there is a lack of a comprehensive inter-comparison due to the availability of quality checked in situ databases. The CoastColour project Round Robin (CCRR) project funded by the European Space Agency (ESA) was designed to bring together a variety of reference datasets and to use these to test algorithms and assess their accuracy for retrieving water quality parameters. This information was then developed to help end-users of remote sensing products to select the most accurate algorithms for their coastal region. To facilitate this, an inter-comparison of the performance of algorithms for the retrieval of in-water properties over coastal waters was carried out. The comparison used three types of datasets on which ocean colour algorithms were tested. The description and comparison of the three datasets are the focus of this paper, and include the Medium Resolution Imaging Spectrometer (MERIS) Level 2 match-ups, in situ reflectance measurements and data generated by a radiative transfer model (HydroLight). These datasets are available from doi.pangaea.de/10.1594/PANGAEA.841950.

The datasets mainly consisted of 6484 marine reflectance associated with various geometrical (sensor viewing and solar angles) and sky conditions and water constituents: Total Suspended Matter (TSM) and Chlorophyll *a* (CHL) concentrations, and the absorption of Coloured Dissolved Organic Matter (CDOM). Inherent optical properties were also provided in the simulated datasets (5000 simulations) and from 3054 match-up locations. The distributions of reflectance at selected MERIS bands and band ratios, CHL and TSM as a function of reflectance, from the three datasets are compared. Match-up and in situ sites where deviations occur are identified. The distribution of the three reflectance datasets are also compared to the simulated and in situ reflectances used previously by the International Ocean Colour Coordinating Group

ESSDD

8, 173–258, 2015

## CoastColour Round Robin datasets

B. Nechad et al.

Title Page

Abstract

Instruments

Data Provenance & Structure

Tables

Figures



Back

Close

Full Screen / Esc

Printer-friendly Version

Interactive Discussion





sets of IOPs and geometrical conditions. MERIS images were also provided for the selected regions where the remote sensing WQ algorithms are tested.

The match-ups, the in situ reflectance and the simulated datasets are presented in Sect. 2, and the variability of WQ is characterized. The data from the three datasets are inter-compared in Sect. 3. This study provides documentation for the publicly available datasets (as detailed in Sect. 4) which can be used as benchmarks for ocean colour algorithm testing in coastal waters, to ultimately improve the remote sensing algorithms.

## 2 Data

The in situ WQ provided in the match-up dataset and referred to hereafter as “match-up field measurements” are described in Sect. 2.1.1. The concurrent MERIS Level2 products, reported in Sect. 2.1.2, include the MERIS reflectances and WQ, denoted respectively as L2R and L2W, and Level 2 flags. The in situ reflectance dataset consists of in situ TSM and CHL measurements collected simultaneously with reflectances that cover the spectral range 440–709 nm. Inclusion of the 709 nm band in these datasets is important because it allows testing of algorithms exploiting this MERIS band which is unique on current ocean colour sensors.

The artificial dataset is based on radiative transfer simulations. The match-up, in situ reflectance and simulated datasets are described respectively in Sects. 2.1, 2.2 and 2.3. These datasets come from 18 research institutes or databases (Table 1).

### 2.1 Match-up dataset

The measurements in the match-up dataset cover various water types from ocean and coastal regions called CoastColour sites, and consist of a collection of biogeochemical and optical measurements (inherent and apparent optical properties, hereafter referred as IOPs and AOPs) along with the associated metadata. Only the WQ for which

Title Page

Abstract

Instruments

Data Provenance & Structure

Tables

Figures



Back

Close

Full Screen / Esc

Printer-friendly Version

Interactive Discussion



remote-sensing algorithms were tested within the CCRR, such as CHL and TSM (see Table 2), are described in this paper, although supplementary oceanographic parameters are also included in the match-up database.

The match-up field measurements were collected at 17 CoastColour sites, selected in the framework of the CCRR (Fig. 1) where in situ WQ from 2005 to 2010 were available, and measured above 5 m depth. MERIS L2R and L2W products from 2005 to 2010, derived at match-up locations, are included in the match-up dataset, but only MERIS L2R are described in this paper.

The temporal availability of these data displayed in Fig. 2 shows unbalanced distributions over the CoastColour sites. The seasonal distribution of the match-up field measurements varies from one site to another (Fig. 3), e.g. for chlorophyll *a* measurements 52 % of Acadia data were collected during the period June–August, 67 % of Chesapeake Bay data during September–November, and 100 % of Benguela data were measured during March–May; the seasonal distribution may also vary within each site between the different WQ. From all the sites, the ensemble of temperature, salinity, chlorophyll *a*, particulate organic matter (PIM), and particulate inorganic matter (POM) measurements is evenly balanced throughout the seasons. During December–February, less TSM, Turbidity, *a*, *a<sub>p</sub>*, *a<sub>phy</sub>*, *a<sub>d</sub>* and *a<sub>g</sub>* measurements are available than during the other periods (about 13 to 18 % of the data), while the quantity of AOP data is significantly lower (2 to 9 % of the data).

### 2.1.1 Match-up field measurements

The number of stations where metadata, biogeochemical, IOP and AOP data were collected over the CoastColour sites are reported in Tables 3a and b. The availability of measurements throughout the sites varies from one parameter to another, e.g. chlorophyll *a* concentration measurements were available from 16 sites while the scattering coefficient spectra were collected at 2 sites.

Metadata including depth, temperature and salinity, exceeded 20 000 for each parameter, whereas the number of bio-geochemical, IOPs and AOPs were much lower:

Title Page

Abstract

Instruments

Data Provenance & Structure

Tables

Figures

◀

▶

◀

▶

Back

Close

Full Screen / Esc

Printer-friendly Version

Interactive Discussion



11 157 chlorophyll *a* concentration measurements, 1213 TSM measurements, 966 reflectance spectra (the other AOP data do not reach 200 data each), and less than 700 IOP data (for each parameter) except for turbidity ( $N = 2162$ ).

5 The number of CHL and turbidity measurements collected at the North Sea site constitutes 77.0 and 99.8 % of the measurements respectively, while smaller amounts of TSM and Rrs data were provided from the North Sea site: 17.5 and 5.6 % of the total CCRR match-up field TSM and reflectance data respectively. When excluding the turbidity data, 91.6 % of the IOP measurements were contributed from the Southern California (38.7 %), North Sea (22.9 %), Florida (7.6 %) and the GBR region (7.0 %) sites.

10 The methods of chlorophyll *a*, TSM, IOPs and Rrs measurements performed by each data contributor are briefly described below. Chlorophyll *a* measurement methods by the different laboratories are summarized in Table 4.

## Chlorophyll *a* and TSM

15 Chlorophyll *a* concentrations were measured either by High-Performance Liquid Chromatography (HPLC), by fluorometry or spectrophotometry. In the following, TChl *a* refers to chlorophyll *a* measurements determined by HPLC and Chl *a* denotes chlorophyll *a* obtained by fluorometry or spectrophotometry. TSM concentrations were collected at nine sites: the E. Md. Sea, the Baltic and E. Md. Seas, The Great Barrier Reef region (referred to hereafter by the GBR region), the Indonesian waters, Morocco-W. Md. Sea, the North Sea, the Red Sea and Tasmania coastal waters.

20 In the CEOAS dataset, 422 TChl *a* data were measured from 2006 to 2009 at the Oregon-Washington site and 2 at the Central California site. Samples were stored at  $-80^{\circ}\text{C}$  until HPLC analysis. The distribution of TChl *a* measurements from Oregon-Washington is seasonally unbalanced with 8 % of the measurements collected during the period of December–February, 38 % in March–May, 50 % in June–August, and 50 % in September–November.

Title Page

Abstract

Instruments

Data Provenance & Structure

Tables

Figures



Back

Close

Full Screen / Esc

Printer-friendly Version

Interactive Discussion



CoastColour Round  
Robin datasets

B. Nechad et al.

Title Page

Abstract

Instruments

Data Provenance &amp; Structure

Tables

Figures



Back

Close

Full Screen / Esc

Printer-friendly Version

Interactive Discussion



The CSIC dataset contains 736 Chl *a* and 667 triplets of TSM, POM and PIM measurements collected in the Gulf of Cadiz (southwest Iberian Peninsula) within the Morocco-W. Md. Sea site. The measurements were taken in the nearshore area (< 30 km) of the Guadalquivir estuary from 2005 to 2007, and offshore during 2008 with slightly lesser measurements during the periods June–August (19 % of the data). Chlorophyll analysis was conducted by filtering samples of 500 mL through Whatman GF/F glass fiber filters (0.7  $\mu\text{m}$  pore size), extracting in 90 % acetone, and measuring chlorophyll *a* by standard fluorometric methods using a Turner Designs Model-10 following JGOFS protocols (IOC/UNESCO, 1996). TSM concentrations were measured gravimetrically on pre-weighted Whatman GF/F (0.7  $\mu\text{m}$  pore size) after rinsing with distilled water, following JGOFS protocols (IOC/UNESCO 1996). Organic matter lost on ignition was determined by reweighting the filters after 3 h in the oven at 500 °C, giving the concentrations of POM and POM (by subtraction).

The CSIR chlorophyll data were collected from the Benguela coastal surface waters and measured using the standard fluorometric method of Parsons (1984) with a Turner Designs Model-10AU fluorometer. A total of 131 Chl *a* measurements were available from March–April of years 2005–2009.

The CSIRO dataset consisted of data collected at 63 stations in the GBR region from 2005 to 2008 (where 25, 19 and 55 % were available from March–May, June–August and September–November respectively) and at 21 stations in the Tasmanian waters in May 2007. Water samples were filtered through Whatman GF/F glass fiber filters with 0.7  $\mu\text{m}$  nominal pore size and stored in liquid nitrogen until analysis by HPLC. The analyses conducted on the dataset collected before July 2004 followed the method of Wright et al., (1991), while the method of Van Heukelem and Thomas (2001) was used for the subsequent campaigns (Oubelkheir et al., 2006; Blondeau-Patissier et al., 2009). For TSM analysis, the filters were pre-ashed at 450 °C, pre-washed in 100 mL of Milli-Q water, dried and pre-weighted. The samples were rinsed with 50 mL distilled water, stored in Petri slide at 4 °C. The filters were dried at 60 °C (van der Linde, 1998).

## CoastColour Round Robin datasets

B. Nechad et al.

Title Page

Abstract

Instruments

Data Provenance & Structure

Tables

Figures

◀

▶

◀

▶

Back

Close

Full Screen / Esc

Printer-friendly Version

Interactive Discussion



The EMECO dataset was provided by the International Council for the Exploration of the seas (ICES) and Smartbuoys data by the Center for Environment, Fisheries and Aquaculture Science (Cefas), totaling 6274 stations where Chl *a* measurements were provided, calibrated by HPLC. The distribution of these measurements is slightly unbalanced between the seasons (29 % of data available during March–May and 19 % in September–November).

The GKSS provided TSM and TChl *a* measurements collected at 48 stations in the North Sea. TChl *a* and TSM measurements follow the protocol described in Doerffer and Schönfeld (2009). The sampling was equally distributed between the periods April–May, June–July and September–October of years 2005–2006 with no measurements during December–February.

The HCMR data were collected at transect stations where samples were taken in Niskin bottles from HCMR RV Aegaeo, in the E. Md. Sea site. For Chl *a* measurements, the filtrations were performed using 47 mm diameter nucleopore of Millipore, membrane polycarbonate, with 0.2 µm nominal pore size; Chl *a* was measured using Turner 00-AU-10 and Turner TD700 fluorimeters using the EPA Method 445 (Holm-Hansen et al., 1965) adapted by Arar and Collins (1992). For TSM measurements, the samples were filtered through 47 mm diameter, 0.45 µm Millipore, membrane isopore filters. After filtration of water samples, the filters were rinsed with Milli-Q to remove salt. The filters were dried in the oven at 60 °C. 294 Chl *a* measurements were collected from 2005 to 2009, where 18 and 32 % were measured during the periods June–August and September–November respectively. TSM measurements were available at 45 stations, sampled during years 2005 and 2008, with 47, 13 and 40 % of data taken during the periods March–May, June–August and September–November respectively.

The Ifremer dataset consisted of 975 Chl *a* measurements collected at 30 different locations within the Armorican Shelf (north-west of France), from 2005 to 2009. Data were available from the French phytoplankton surveillance network (REseau PHYtoplankton, REPHY). Fluorometric measurements of Chl *a* were performed mostly in laboratory using a Turner C7 and C3. For the four periods (seasons) from December–

February to September–November, 18, 27, 32 and 23 % of the measurements were sampled respectively.

The ITC measurements of Chl *a* and TSM were carried out in the Mahakam Delta waters from the upstream turbid Mahakam River down to the clear water situated in the seaward area influenced by the Makassar Strait. The measurements covered the wet (May) and dry (August) seasons in 2008 and during the dry season in August 2009, with total 119 stations. From each station, two 1 L bottles of surface water samples were taken, and stored onboard in cool and dark conditions until their processing in the laboratory. TSM concentrations were determined using the gravimetric method. Water samples were filtered through previously weighted 47 mm diameter filters (Whatman GF/F filters, pore size of 0.45 µm). The filters were dried and reweighed (Clesceri et al., 1998). Chl *a* concentrations were measured using a spectrophotometer after the water samples had been filtered through 47 mm diameter filters (membrane filter, pore size of 0.45 µm) (Clesceri et al., 1998).

The KORDI dataset included 47 Chl *a* and 78 TSM measurements collected at the East China Sea site. Samples were filtered through a 25 mm diameter GF/F fiberglass filter. Chl *a* measurements were performed through the methanol-extraction method using a Perkin–Elmer Lambda 19 dual-beam spectrophotometer. TSM and Chl *a* data were available from cruises carried out during April and June 2007 and April 2009, and 31 TSM data were available from measurements made in July 2006. 41 and 59 % of TSM measurements were available during the periods of April–May and June–July respectively, while 68 and 32 % of Chl *a* data were provided for these periods.

The NOAA Chl *a* data were based on in vitro fluorescence measurements following dark-24 h extractions in acetone. A total of 136 measurements were available from the Oregon–Washington site sampled from July to September 2008; 122 Chl *a* data from Southern California acquired during the period September–November in 2008; and 606 Chl *a* data from Central California site, measured from 2005 to 2010. 52 and 30 % of the NOAA Chl *a* collection were available from the periods of September–November and June–August respectively.

## CoastColour Round Robin datasets

B. Nechad et al.

Title Page

Abstract

Instruments

Data Provenance & Structure

Tables

Figures



Back

Close

Full Screen / Esc

Printer-friendly Version

Interactive Discussion



## CoastColour Round Robin datasets

B. Nechad et al.

Title Page

Abstract

Instruments

Data Provenance & Structure

Tables

Figures

◀

▶

◀

▶

Back

Close

Full Screen / Esc

Printer-friendly Version

Interactive Discussion



The NASA bio-optical Marine Algorithm Dataset (NOMAD) presents a large collection of bio-optical data in ocean and coastal waters (Werdell and Bailey, 2005). The NASA SeaWiFS Bio-optical Archive and Storage System (SeaBass, (Werdell et al., 2003)), included in the NOMAD dataset, combines both the HPLC and fluorometric methods. HPLC methods may differ between laboratories, to separate different types of pigments, which may depend on the predominant component of chlorophyll (Hooker et al., 2005). HPLC derived TChl *a* in the NOMAD dataset are the sum of monovinyl and divinyl chlorophyll *a*, plus chlorophyllide-*a*, allomers and epimers (Werdell and Bailey, 2005). The NOMAD dataset provided TChl *a* constituted 24 % of the total TChl *a* measurements gathered within the CoastColour match-up dataset. From 2005 to 2007, 175 TChl *a* were collected from the six CoastColour sites: Acadia (40 data), Chesapeake Bay (69), Gulf of Mexico (41), Indonesian waters (4), Southern California (16) and Trinidad and Tobago (5) and 142 Chl *a* measurements were available from Acadia (25 data), Chesapeake Bay (12), Florida (84), Gulf of Mexico (6), Indonesian waters (4) and Trinidad and Tobago (11).

The PML dataset was collected during RV and JCR cruises in MOS-2 and L4 areas respectively. The extraction of chlorophyll was performed in acetone including apocarotenolate and the separation used reverse phase HPLC, during 30 s sonification, and 5 min centrifugation (4000 rpm) (Barlow et al., 1997). In the PML dataset, divinyl-chlorophyll *a*, chlorophyllide *a* and chlorophyll *a* isomers and epimers are added to chlorophyll *a* (Barlow et al., 1997). For TSM measurements, 2 to 4 L seawater samples were filtered in triplicates, washed with Milli-Q. Filters were pre-ashed at 450 °C for four hours, pre-washed in 500 mL of Milli-Q water, oven-dried at 75 °C for 24 h, and pre-weighted (van der Linde, 1998). A total of 191 pairs of Chl *a* and TChl *a* and 136 TSM measurements were collected by PML between 2005 and 2009. The distributions of Chl *a*, TChl *a* and TSM measurements are overall well balanced across seasons.

The UNICAN dataset included 28 TSM and Chl *a* measurements collected in the North Sea region (the Bay of Biscay) in July 2010. Chl *a* was measured through a Hach Lange DR-5000 with Whatman GF/F filter following the spectrophotometric method de-

scribed in Standard Methods (trichromatic method), using a white reference to control the quality of the measurements. TSM was estimated using a gravimetric method after filtration through GF/C fiberglass filters.

### Inherent optical properties

IOP measurements were collected at 11 sites (blue symbols in Fig. 2). The measurement methods for the total absorption coefficient,  $a$ , absorption by CDOM,  $a_g$ , by particles,  $a_p$ , by detritus,  $a_d$ , and by phytoplankton pigments,  $a_{phy}$ , the scattering  $b$  and backscattering coefficients  $b_b$ , and the total beam attenuation coefficient,  $c$ , and particles beam attenuation,  $c_p$ , are briefly described below.

For the CSIRO measurements of  $a$ ,  $a_p$  and  $a_{phy}$ , carried in the GBR region and Tasmania coastal waters, samples were filtered using a 25 mm Whatman GF/F filter with 0.7  $\mu\text{m}$  nominal pore size, and stored in liquid nitrogen (Oubelkheir et al., 2006; Blondeau-Patissier et al., 2009). CDOM absorption was determined after filtration through polycarbonate filters (Millipore), of 0.22  $\mu\text{m}$  nominal pore size, water samples were filtered immediately after collection, stored in cool and dark conditions until analysis (Tilstone et al., 2002). The backscattering coefficients were measured using HOBI Labs HydroScat-6. The spectral dependency of the scattering coefficient was modeled as a hyperbolic, using bands 412, 488, 510, 532, 555 and 650 nm (Oubelkheir et al., 2006; Blondeau-Patissier et al., 2009).

In the HCMR dataset collected in the E. Md. Sea, 139 measurements of  $c_p$  were provided at 470, 660 and 670 nm (available at least at one of these wavelengths), and 34 measurements of  $c_p$  given at 670 nm. The beam attenuation coefficients were measured using a 0.25 m path length transmissometer Chelsea Technologies Group Ltd. Alpha Tracka II, emitting at 470 nm. The instrument was mounted on the RV's permanent CTD rosette frame for casts through the water column. The data were quality-controlled, filtered, and binned at 1 m intervals (Karageorgis et al., 2012).

MSU provided 6 measurements of  $a$ ,  $b$  and  $c$  coefficients collected at the Gulf of Mexico site.

## CoastColour Round Robin datasets

B. Nechad et al.

Title Page

Abstract

Instruments

Data Provenance & Structure

Tables

Figures

◀

▶

◀

▶

Back

Close

Full Screen / Esc

Printer-friendly Version

Interactive Discussion



CoastColour Round  
Robin datasets

B. Nechad et al.

Title Page

Abstract

Instruments

Data Provenance &amp; Structure

Tables

Figures

◀

▶

◀

▶

Back

Close

Full Screen / Esc

Printer-friendly Version

Interactive Discussion



The NOMAD absorption coefficients  $a_p$  and  $a_g$ , and absorption by detritus  $a_d$ , were derived by spectroscopy at six CoastColour sites (Acadia, Cape Verde, Florida, Indonesian waters, Morocco-W. Md. Sea and Southern California). Note that for the Indonesian waters, only  $a_g$  was provided. These data have been quality controlled, removing unreasonable data and instrument artifacts (Werdell, 2005). The spectral backscattering coefficient provided in NOMAD dataset was obtained using HOBI Labs HydroScat  $a\beta$  and  $c\beta$  sensors, WETLabs  $ECO_b$  and  $ECOVSF$  sensors, and Wyatt Technology Corporation DAWN photometers. The details on  $b_b$  data processing are given in Werdell (2005).

Absorption coefficient spectra were measured by PML at 5 m depth in the North Sea, using the WET Labs ac9+. As reported in Martinez-Vicente et al. (2010), the measurements were corrected to account for temperature, salinity and scattering effects. The samples were filtered through 47 mm diameter Whatman Anopore membranes (0.2  $\mu$ m pore size), using pre-ashed glassware. Absorption coefficients were determined on the spectrophotometer and a 10 cm quartz cuvette from 350 to 750 nm, relative to bi-distilled Milli-Q reference blank.  $a_g$  was calculated from the optical density and the cuvette pathlength and baseline offset was subtracted from  $a_g$  (Groom et al., 2009). The measurement of  $a_{phy}$  followed the method of Tassan and Ferrari (1995). The coefficients  $a_p$  and  $a_{phy}$  were measured using a Perkin–Elmer Lambda-2 spectrophotometer, and 25 mm GF/F filters (Tilstone et al., 2012).  $a_p$  were determined before and after pigment extraction using NaClO 1 % active chloride from 350 to 750 nm. The scattering measurements were performed using an  $ECO$  VSF-3 sensor (Martinez-Vicente et al., 2010).

The backscattering measurements from USCB were performed using HOBI Labs HydroScat-6, and collected at the Southern California site, with a total of 270 spectra given at 442, 470, 510 and 589 nm.

## Apparent optical properties: water-leaving reflectance

A total of 957 match-up field RLw spectra were collected at 13 CoastColour sites and provided from eight Data Providers, covering a variety of time periods as listed in Table 5. About 33% of these data were provided for the Southern California region, 13% for the Indonesian coastal waters site, 9% for the Benguela and Florida sites, and 8% from the Acadia and Chesapeake Bay sites. Less than 19% of the dataset was provided from the rest of the CoastColour sites. Hyperspectral RLw were measured in the GBR region, the North Sea and the Indonesian waters.

The instruments and methods of RLw measurements are summarized in Table 6 and briefly described below.

The CEOAS radiometric measurements in the Oregon-Washington site were performed using a Satlantic HyperPro II instrument, equipped with two hyperspectral sensors to vertically profile the upwelling radiance,  $L_u$ , and downwelling irradiance,  $E_d$ , in the water column, plus a separate surface sensor mounted high on the ship deck that measures the above-water downwelling irradiance,  $E_s$ . Processing of the collected data was performed using Satlantic ProSoft software version 8.1.3\_1 (see <http://satlantic.com/sites/default/files/documents/ProSoft-7.7-%20Manual.pdf> for equations). In summary, the above-water radiance  $L_w$  is calculated by extrapolating the profiled  $L_u$  measurements to the subsurface ( $L_u(0^-)$ ) and then accounting for the air-sea interface:  $L_w = L_u(0^-)(1 - \rho)/n_w^2$  where  $\rho$  is the Fresnel reflectance of the air-sea interface (set to 0.021) and  $n_w = 1.345$  is the refractive index of seawater. The surface irradiance reflectance is then obtained by  $RLw = \pi L_w / E_s$ . Of the 137 wavelengths measured by the HyperPro II, this study presents data from 21 wavelengths covering 412 to 780 nm for RLw.

In the Benguela site, the CSIR used a Satlantic radiometer mounted on a floating buoy attached to the ship, to measure the upwelling radiance  $L_u$  and the downwelling irradiance  $E_d$  at 0.66 m below the water surface.  $L_u$  was extrapolated to  $L_w$  by means of the upwelling diffuse attenuation coefficient,  $K_u$ , as described by Albert and Mobley

ESSDD

8, 173–258, 2015

### CoastColour Round Robin datasets

B. Nechad et al.

Title Page

Abstract

Instruments

Data Provenance & Structure

Tables

Figures

◀

▶

◀

▶

Back

Close

Full Screen / Esc

Printer-friendly Version

Interactive Discussion



(2003). RLw was estimated from Lw and Ed using a reflectance inversion algorithm optimized for local conditions.

The CSIRO RLw measurements in the GBR region were conducted under stable clear sky conditions using one TriOS RAMSES instrument. Subsequent water-leaving radiance, Lw, sky radiance, Lsky and spectralon upwelling radiance, Lspec were measured. Irradiance was calculated from spectralon measurements according to  $Ed = \pi L_{spec} C$  where  $C$  is the reflectance correction factor accounting for non-perfect Lambertian panel properties. Water-leaving reflectance was calculated according to the REVAMP protocol (Tilstone et al., 2002) by applying a sky correction factor.

The GKSS radiometric measurements were conducted onboard ferry cruises in the North Sea region, using three TriOS Ramses radiometers that measure simultaneously Lu at 45° viewing angle, Es and Lsky, with an azimuth angle between 130 and 140° relative to the sun. The water-leaving reflectance RLw was computed according to  $RLw = \pi(Lu - \rho_{sky} Lsky) / Ed$  where the specular reflectance  $\rho_{sky}$  is computed using the Fresnel law, as a function of the refractive index for the mean salinity along the transect.

The ITC measurements carried out in the Indonesian waters used two TriOS Ramses spectroradiometers. The surface water upwelling and sky downwelling radiance measurements, Lu and Lsky, were measured sequentially at 40° zenith angle and at 40° nadir angle respectively. The irradiance sensor was mounted on an aluminum pole on top of the boat, pointing upward. The boat was positioned on a station to point the radiance sensor at a relative azimuth angle of 135° away from the sun. The sensors measured over the wavelength range 350–950 nm with a sampling interval of approximately 3.3 nm. The measurements were conducted during different cloud conditions. The sky radiance reflected by the water surface,  $\rho_{sky}$ , was estimated by assuming very small (but not zero) water-leaving reflectance in the near-infrared and that  $\rho_{sky}$  values were less than 0.07 which is the highest value of scattered cumulus clouds by Mobley (1999). The result of  $\rho_{sky}$  values were relatively similar with  $\rho_{sky}$  values given by Mobley (1999) for each cloud type condition. The water-leaving reflectance was obtained following equation  $RLw = \pi(Lu - \rho_{sky} Lsky) / Ed$ .

CoastColour Round Robin datasets

B. Nechad et al.

Title Page

Abstract

Instruments

Data Provenance & Structure

Tables

Figures



Back

Close

Full Screen / Esc

Printer-friendly Version

Interactive Discussion



The MSU radiometric measurements were provided for the Gulf of Mexico in the Mississippi Sound area (around Gulfport). The reflectance spectra were provided at 14 wavelengths in the spectral range 380–780 nm.

From the NOMAD database, Lw and Es measurements were extracted for the match-up locations between 2005 and 2010, and converted to RLw spectra. Various methods and instruments were used for the measurements of the remote-sensing reflectance, Rrs, in the NOMAD dataset (Werdell and Bailey, 2005), including in-water profiling or above-water measurements. As mentioned in (Werdell and Bailey, 2005), the water-leaving radiance was estimated from Rrs using Es when the incident irradiances were provided, or assuming a clear sky model based on Frouin et al. (1989).

### 2.1.2 MERIS data

MERIS CoastColour processing (see flow chart in Fig. 4) is applied to MERIS Level 1 Full Resolution Swath (FRS) to produce MERIS Level 2 match-up datasets, namely MERIS water-leaving reflectance (L2R) and MERIS water quality products (L2W), over the CoastColour sites. Here, a brief description of MERIS CoastColour processing is given.

MERIS FRS products including auxiliary data such as surface pressure, ozone, geographical location (used to identify products having an overlap with one of the test sites), viewing and sun angles and solar flux, are processed with the Accurate MERIS Ortho-Rectified Geolocation Operational Software (AMORGOS processor, developed by ACRI –Earth Observation, Environment within ESA GlobCover project), yielding geometrically corrected MERIS child products (FSG). The L1P processor subsamples the FSG data, applies the radiometric and smile corrections and performs equalization following Bouvet and Ramoino (2010) and pixel classification, screening cloud pixels.

The L1P product, which contains the top of atmosphere radiance reflectance (TOA), is then atmospherically corrected to determine the water-leaving radiance reflectance, following the steps described in Doerffer (2001) which yields the L2R products. Furthermore, water pixels are classified according to their TOA reflectances and available

## CoastColour Round Robin datasets

B. Nechad et al.

Title Page

Abstract

Instruments

Data Provenance & Structure

Tables

Figures



Back

Close

Full Screen / Esc

Printer-friendly Version

Interactive Discussion



geographical information, and L2W products are generated using various ocean colour algorithms. The complete list of the parameters contained in L2R and L2W products are given in Table 7.

Boxes of  $5 \times 5$  pixels are extracted from L1P, L2R and related L2W products at all match-up locations present for a given test site and are stored in three files associated with the site. Further processing is performed to average MERIS L2R spectra in each  $5 \times 5$  box, discarding low quality pixels (see the list of critical flags in Table 7), and yielding the mean reflectance denoted hereafter as MERIS RLw, and its SD. Other L2W and atmospheric products are also averaged over the  $5 \times 5$  box (see the list in Table 8).

Finally, around each match-up location MERIS L1P, L2R and L2W subscenes are provided in BEAM-DIMAP (“dim”) format, and are associated to a kmz file for quick visualization of area location via Google Earth.

With respect to the match-up field RLw dataset, the MERIS RLw dataset included supplementary data from the following regions: the Central California, E. Md. and East China Seas, Central California and Tasmania coastal waters, and extended data from Morocco-W. Md. and the North Seas concurrent with extra match-up field WQ measurements (IOPs and/or biogeochemical datasets). The MERIS RLw dataset was not available for all the locations of the match-up field RLw measurements (e.g. Benguela, Indonesian waters, GBR region), either because no MERIS image was available within 1 h of the match-up field measurement, or MERIS pixels were flagged as cloud, land, suspect, sunglint or invalid. After rejection of the flagged pixels, 457 MERIS RLw spectra remained from the CoastColour sites. About 80 % of these spectra were available from the North Sea region and match in situ measurements of temperature, salinity and/or turbidity.

## 2.2 In situ reflectance dataset

The in situ reflectance dataset comprises a set of 336 RLw spectra sampled at nine MERIS bands from 412 to 709 nm, and collected simultaneously with CHL and/or TSM

## CoastColour Round Robin datasets

B. Nechad et al.

Title Page

Abstract

Instruments

Data Provenance & Structure

Tables

Figures



Back

Close

Full Screen / Esc

Printer-friendly Version

Interactive Discussion





CoastColour Round  
Robin datasets

B. Nechad et al.

Title Page

Abstract

Instruments

Data Provenance &amp; Structure

Tables

Figures

◀

▶

◀

▶

Back

Close

Full Screen / Esc

Printer-friendly Version

Interactive Discussion



characteristics as presented in Table 10, and the specific IOPs (SIOP) for mineral particles (denoted by MP), phytoplankton and  $a_g(443)$  as given in Table 11. The SIOPs include the specific absorption coefficients for phytoplankton,  $a_p^*$ , and for MP,  $a_{MP}^*$ , and the spectral slope of  $a_{MP}^*$ , denoted by  $S_{MP}$ , the specific scattering coefficient for MP,  $b_{MP}^*$ , the spectral variation of the beam attenuation coefficient for phytoplankton,  $\gamma_{CHL}$ , and for MP,  $\gamma_{CMP}$ , and the spectral slope of CDOM absorption,  $S_{CDOM}$ .

This simulated dataset is denoted as “CCRRv1” to facilitate comparison with future versions, e.g. with variability of the specific inherent optical properties.

A total of 5000 triplets of CHL and MP concentrations and  $a_g(443)$  were generated according to the following:

- a random number function modelling a log-normal probability density function was used for CHL
- the associated MP and  $a_g(443)$  values were also generated by a random number function but constrained to yield reasonable covariation of the triad, comparable to that reported by Babin et al., (2003b) from in situ measurements in coastal European waters.

Figure 5a and b shows the distributions of the simulated MP and  $a_g(443)$  vs. CHL concentrations and their co-variations.

Based on these concentrations and SIOP models, a set of hyperspectral (2.5 nm resolution) data were generated including the total absorption,  $a$ , scattering,  $b$ , and backscattering,  $b_b$ , coefficients, phytoplankton absorption coefficient,  $a_{phy}$ , and the ratio  $b_b/a + b_b$ . For each in-water content (5000 cases) and sun angle (3 cases), Hydrolight computed RLw and the diffuse downwelling irradiance attenuation spectra,  $K_d$ , as well as the Photosynthetically Available Radiation, PAR. The spectra were further spectrally subsampled to (a) MERIS bands central wavelengths: 412.5, 442.5, 490, 510, 560, 620, 665, 681.25, 708.75, 753.75, 761.875, 865, 885 and 900 nm, (b) MODIS bands: 412, 443, 469, 488, 531, 547, 645, 667, 678, 748, 859 and 869 nm and (c) SeaWiFS

bands: 412, 443, 490, 510, 555, 670, 765 and 865 nm. In the following, only spectra generated at MERIS bands are presented.

### 3 Results and discussion

The distributions of water depth, temperature and salinity, CHL and TSM concentrations, IOPs and AOPs are presented in the next Sects. 3.1–3.6, followed by the analysis of the covariation between CHL and TSM and bio-optical relationships existing in the CCRR datasets (Sect. 3.7).

The distributions of CHL, TSM and IOPs in the match-up field dataset and the in situ reflectance dataset are related to the AOPs measured throughout the CoastColour sites. The similarities/differences in these relationships characteristic of these sites may shed light on the common (universal) bio-optical relationships and/or emphasize some more regional features, which is of interest for remote sensing algorithm development and validation. The bio-optical relationships within the match-up field and in situ datasets are also compared to the models assumed in the simulated CCRRv1.

#### 3.1 Water depth, temperature and salinity

The CoastColour sites are characterized by different distributions of water depth, temperature and salinity (Fig. 6). The median water depth varies from 2 m in the Gulf of Mexico to more than 1000 m in the Morocco-W. Md. Sea, Trinidad and Tobago, E. Md. Sea, Southern California and Cape Verde sites (Fig. 6a). The sea surface temperature in the North Sea ranges from  $-0.6$  to  $26$  °C, encompassing the ranges of temperature reported at the four other sites (Fig. 6b), probably due to the quasi-continuous sampling in the North Sea throughout the cold and warm seasons (Fig. 2). The frequent sampling of salinity in the North Sea across seasons is exhibited in the large range of this measurement (0.5–37 psu). About 82 % of salinity data measured in the CoastColour sites exceeds 32 psu (Fig. 6c).

## CoastColour Round Robin datasets

B. Nechad et al.

Title Page

Abstract

Instruments

Data Provenance & Structure

Tables

Figures



Back

Close

Full Screen / Esc

Printer-friendly Version

Interactive Discussion



Note however that these distributions may not represent all the conditions within which the entire in situ measurements were collected, since the time windows of the metadata (excluding the date, time and geographic coordinates) do not always cover those of the measurement of the biogeochemical data, IOPs and AOPs (Figs. 2 and 3).

### 3.2 Chlorophyll *a* concentration

TChl *a* (HPLC method) and Chl *a* (fluorometric method) span from 0 to extremely high values ( $> 1000 \text{ mg m}^{-3}$ ) in the Central California site (Fig. 7a and b). TChl *a* values vary by about 2 orders of magnitude in most of the sites. The low number of TChl *a* measurements ( $\leq 5$ ) in the data from the Indonesian waters and Trinidad and Tobago sites may explain the reduced variability observed there. With the higher number (temporal and spatial coverage) of Chl *a* measurements, larger ranges of variability are found in the measurements from the Indonesian waters and about 7 orders of magnitude from the measurements taken in the Central California site. For most of the sites, Chl *a* varies at least 3 orders of magnitude.

Chlorophyll *a* concentrations (either Chl *a* or TChl *a*) exhibit median values less than  $1 \text{ mg m}^{-3}$  from the E. Md. Sea, GBR region, Morocco-W. Md. Sea, Tasmania and Trinidad and Tobago sites. Some of these sites have been extensively studied, and characterized as ultra to oligotrophic ( $\text{CHL} \leq 1 \text{ mg m}^{-3}$ ), or mesotrophic to eutrophic waters:

- The eastern Mediterranean Sea is oligotrophic due to nutrient limitations. CHL ranges from  $\sim 0.02 \text{ mg m}^{-3}$  in the Cyprus eddy to  $0.3 \text{ mg m}^{-3}$  during the winter bloom (Groom et al., 2005). Similar ranges of CHL were reported in the ultra-oligotrophic eddies of the western Mediterranean Sea (Loisel et al., 2011).
- In the GBR region the water composition is largely influenced by the land use in the adjacent catchments (Schaffelke et al., 2012). Chlorophyll *a* concentra-

Title Page

Abstract

Instruments

Data Provenance & Structure

Tables

Figures

◀

▶

◀

▶

Back

Close

Full Screen / Esc

Printer-friendly Version

Interactive Discussion





in the Columbia River Plume. It is also possible that variability in the dataset is due to slight differences in sampling protocols between the laboratory groups although this would likely be minimal.

In Chesapeake Bay, a distribution similar to the match-up data was described in Tzortziou et al. (2007) based on measurements performed in 2001 where the mean CHL value was about  $15 \text{ mg m}^{-3}$ , and higher CHL values up to  $74 \text{ mg m}^{-3}$  occurred during spring and summer periods.

Overall, the chlorophyll *a* match-up dataset collected for the CCRR exercise are representative of the distributions reported in literature. Moreover, the measured Chl *a* and TChl *a* in the CoastColour sites show a high correlation ( $r = 96.2\%$ ,  $N = 402$ ) with mean absolute percentage error (MAPE) equal to  $11.5\%$  (Fig. 7c). Most of the discrepancy between TChl *a* and Chl *a* are noticed in measurements from the Southern California site. When this site is excluded, a significantly lower MAPE is obtained for the seven sites (MAPE =  $3.6\%$  with correlation  $r = 99.8\%$ ).

### 3.3 TSM, turbidity, Kd and Kpar

The distributions of TSM are reported in Fig. 8a. PIM and POM concentrations were also measured (over three and four CoastColour sites respectively) and their distributions are indicated in the bottom panel of Fig. 8b and c.

The measurements from the E. Md. Sea show the lowest TSM concentrations (TSM  $< 1 \text{ g m}^{-3}$ ,  $N = 45$ ), whereas Morocco-W. Md. Sea exhibits the highest values (median TSM  $> 20 \text{ g m}^{-3}$ ,  $N = 667$ ) associated mainly with inorganic matter as indicated by the high values of PIM similar to those of TSM. In Tasmania, TSM varies between  $0.1$  and  $2 \text{ g m}^{-3}$  (Cherukuru et al., 2014). The median TSM concentrations observed from the E.Md. Sea, East China Sea, Tasmania, North Sea, GBR region, Indonesian waters and Morocco-W. Md. Sea sites were  $0.2$ ,  $0.6$ ,  $0.7$ ,  $0.9$ ,  $3.8$ ,  $26$  and  $35.2 \text{ g m}^{-3}$  respectively.

Turbidity measurements were provided at two sites (see Fig. 9a). While the distribution of turbidity matches that of TSM over the North Sea – likely due to significantly

Title Page

Abstract

Instruments

Data Provenance & Structure

Tables

Figures

◀

▶

◀

▶

Back

Close

Full Screen / Esc

Printer-friendly Version

Interactive Discussion



overlapping periods where TSM and turbidity measurements were collected (see the green and red colours in Fig. 2), it presents a significant shift towards lower values, with regard to the high TSM observed earlier in Morocco-W. Md. Sea. This is likely due to the significantly lower number of turbidity sampling periods (only 2 cruises).

The ranges of  $K_d(443)$  and  $K_{par}$  measurements (Fig. 6c and d) show similar differences amongst the Acadia, Cape Verde, Chesapeake Bay, Indonesian waters, Morocco-W. Md. Sea, North Sea, Southern California and Trinidad and Tobago sites: the highest mean values are observed in Acadia and Chesapeake Bay (corresponding to the lowest mean values of  $Z_{1\%} < 20$  m, see Fig. 9b), and the lowest in Cape Verde, Morocco-W. Md. Sea and the Indonesian waters, which correspond to the highest mean values of  $Z_{1\%} > 60$  m found at these three sites. The noticeable shift between  $K_d$  (or  $K_{par}$ ) in Acadia and Cape Verde may be partly explained by the different Chl  $a$  ranges: around  $0.2 \text{ mg m}^{-3}$  in Cape Verde and  $2 \text{ mg m}^{-3}$  in Acadia (Fig. 7a).

### 3.4 CHL vs. TSM

The co-variation of CHL with TSM from the in situ reflectance dataset at 159 locations (where both CHL and TSM are available), was compared to the co-variation of CHL with TSM from the match-up field dataset at 1062 locations. Both co-variations can be visually compared to that of CHL vs. TSM from the simulated dataset (Fig. 10a). The distribution of the ratio CHL/TSM is shown for the match-up field measurements (Fig. 10b).

Except for the data collected in the Morocco-W. Md. Sea, the co-variations of CHL and TSM are generally consistent for the majority of in situ and match-up test sites, showing a general tendency of CHL increasing with TSM, as reported in Babin et al. (2003b, their Fig. 2). The simulated data fit better the distributions of CHL and TSM collected in the North Sea, since their models adopted the distributions documented in Babin et al. (2003b), based on measurements taken in European coastal waters including the North Sea.

Title Page

Abstract

Instruments

Data Provenance & Structure

Tables

Figures

◀

▶

◀

▶

Back

Close

Full Screen / Esc

Printer-friendly Version

Interactive Discussion



CoastColour Round  
Robin datasets

B. Nechad et al.

Title Page

Abstract

Instruments

Data Provenance &amp; Structure

Tables

Figures

◀

▶

◀

▶

Back

Close

Full Screen / Esc

Printer-friendly Version

Interactive Discussion



As previously reported in Sects. 3.2 and 3.3, various CHL and TSM ranges were observed in the match-up field measurements throughout the CoastColour sites (the GBR region, Morocco-W. Md. Sea, the North Sea and Tasmania coastal waters). The in situ reflectance dataset showed differences in CHL and TSM ranges between the Indonesian waters, the North and the Mediterranean Sea. The scatterplot of CHL vs. TSM measured at the Morocco-W. Md. Sea site differs significantly from the other CoastColour sites, due to the occurrence of regularly high TSM (90 % of TSM measurements span between 31.1 and 48.3  $\text{g m}^{-3}$ ) from the Guadalquivir estuary flow, which limits the light available in the water column (Caballero et al., 2014). 90 % of CHL measurements range between 0.08 and 3.1  $\text{mg m}^{-3}$  being the highest in the period March–May and the lowest in later summer. The Guadalquivir River is the main contributor to the continental nutrients discharged in this area, which, combined with episodes of upwelling and rainfall, enables for non-nutrient limited phytoplankton blooms (Prieto et al., 2009).

The simulated data encompasses all the ranges covered by the in situ CHL and TSM (from the in situ reflectance dataset), and partially the ranges of the match-up field data: excluding the outlying distribution of CHL vs. TSM observed in Morocco-W. Md. Sea and few measurements collected in the Indonesian waters and GBR region sites associated to very low CHL/TSM ratio (see Fig. 10b).

Large variability of the ratio CHL/TSM from the match-up field measurements is noticeable amongst the six CoastColour sites, spanning over 5-orders of magnitude (see Fig. 10b). The Morocco-W. Md. Sea site presents the lowest median value of the ratio CHL/TSM ( $< 0.02 \text{ mg}[\text{CHL}]^{-1} \text{ g}^{-1}$ ), being 10 times lower than the median magnitudes measured in the GBR region and Indonesian coastal waters (from 0.1 to 0.2  $\text{mg}[\text{CHL}]^{-1} \text{ g}^{-1}$ ) and about 100 times lower than in the North Sea and Tasmania (around 1.4 and 1.1  $\text{mg}[\text{CHL}]^{-1} \text{ g}^{-1}$  respectively). The East China Sea site exhibits the highest median value of CHL/TSM of 2  $\text{mg}[\text{CHL}]^{-1} \text{ g}^{-1}$ .

Identical CHL and TSM data (92 pairs) from the Indonesian waters are available both in the in situ reflectance dataset and the match-up field measurements, giving identical distributions of CHL vs. TSM and CHL/TSM ratio. From the Mediterranean

CoastColour Round  
Robin datasets

B. Nechad et al.

Title Page

Abstract

Instruments

Data Provenance &amp; Structure

Tables

Figures

I ◀

▶ I

◀

▶

Back

Close

Full Screen / Esc

Printer-friendly Version

Interactive Discussion



Sea, the in situ reflectance dataset collected during March 2009 shows a median value of CHL/TSM of  $1.2 \text{ mg[CHL]}^{-1} \text{ g}^{-1}$ , extending the range of variability of CHL/TSM over 5 orders of magnitudes in the region of Morocco-W. Md. Sea. From the North Sea site, the distribution of CHL/TSM ratios in the in situ reflectance dataset (60 data) was slightly shifted towards lower values relative to the ratios estimated from the match-up field measurements (202 data).

### 3.5 Inherent optical properties

The match-up field absorption coefficient spectra can be classified into four groups, starting from the sites where the lowest amplitudes around 443 nm are observed, to the highest amplitudes: (a) Morocco-W. Md. Sea, Cape Verde and the Indonesian waters sites (Fig. 11), (b) the North Sea (Fig. 12), (c) the GBR region, Acadia and Tasmania sites (Fig. 13); and (d) the Southern California and Florida sites (Fig. 14). All the absorption coefficient spectra exhibit a large variability at shorter wavelengths (around 443 nm, denoted by 44X to refer to 440, 442 or 443 nm) and for  $a_p$  and  $a_{\text{phy}}$  around the phytoplankton absorption peak at 665 nm.

The median values for the available  $a_{\text{phy}}(44X)$  data span between  $0.01 \text{ m}^{-1}$  in the Morocco-W. Md. Sea and Cape Verde sites and  $0.1 \text{ m}^{-1}$  in the Florida site (Fig. 15a). The median values encountered in the GBR region, North Sea and Tasmania are between  $0.031$  and  $0.039 \text{ m}^{-1}$ . Note that the median concentrations of chlorophyll *a* from the GBR region and Tasmania sites are comprised between  $0.4$  and  $0.6 \text{ mg m}^{-3}$ , being 2 to 3 times lower than in the North Sea ( $1.3 \text{ mg m}^{-3}$ ). This indicates that, on average (for the available measurements sampled), the chlorophyll-specific absorption coefficients around 443 nm from the North Sea were lower than from the other two sites (as a comparison see spectra in Tilstone et al. (2012) for the North Sea and Blondeau-Patissier et al. (2009) for Australia). The different periods of sampling relative to the algal bloom events in each site (Fig. 3) may partly explain this general discrepancy between the  $a_{\text{phy}}^*(44X)$  data.

CoastColour Round  
Robin datasets

B. Nechad et al.

Title Page

Abstract

Instruments

Data Provenance &amp; Structure

Tables

Figures

I◀

▶I

◀

▶

Back

Close

Full Screen / Esc

Printer-friendly Version

Interactive Discussion



For  $a_p(44X)$  data, the median values are  $0.012$  and  $0.016 \text{ m}^{-1}$  in Morocco-W. Md. Sea and Cape Verde sites respectively (Fig. 15b). Sensitively higher median values are observed from the North Sea data ( $0.044 \text{ m}^{-1}$ ), Tasmania ( $0.078 \text{ m}^{-1}$ ) and the GBR region ( $0.083 \text{ m}^{-1}$ ), and exceed  $0.1 \text{ m}^{-1}$  in the Florida and Southern California sites.

The coefficients  $a_g$  taken around  $443 \text{ nm}$  and at  $665 \text{ nm}$  span respectively over 3 and 4 orders of magnitude throughout the CoastColour sites (Fig. 15c and d). The Florida measurements exhibit the highest median values around  $443 \text{ nm}$ , exceeding  $0.2 \text{ m}^{-1}$  with a high median value of  $0.006 \text{ m}^{-1}$  at  $665 \text{ nm}$ . Inversely, the Southern California measurements show the highest median value of  $a_g$  around  $665 \text{ nm}$  exceeding  $0.007 \text{ m}^{-1}$ , with a significantly low median value of  $0.05 \text{ m}^{-1}$  at  $443 \text{ nm}$ . Note the overall similar distributions of  $a_g(443)$  from the GBR region and the North Sea sites (median values around  $0.07 \text{ m}^{-1}$ ), while  $a_g(665)$  shows a significant shift towards higher values in the data from the GBR region. The Tasmania data contain two extreme spectra of  $a_g$  (see Fig. 13) which slightly increases the median value for this site up to  $0.09 \text{ m}^{-1}$ , above the value observed in the GBR region.

The ratio  $a_{\text{phy}}(44X)/a_{\text{phy}}(665)$  shows the lowest median value of  $2.7$  in the North Sea and the highest value of  $4.6$  in the GBR region (Fig. 15e), which is inversely related to the distribution of CHL/TSM: the highest median value of CHL/TSM of  $1.5$  ( $\text{mg}[\text{CHL}]^{-1} \text{g}^{-1}$ ) is observed in the North Sea (Fig. 10b), while a lower value of  $\sim 0.1$  ( $\text{mg}[\text{CHL}]^{-1} \text{g}^{-1}$ ) is found in the GBR region.

The distributions of  $a_{\text{phy}}/a_p(440)$  in the GBR region, North Sea and Tasmania sites (see Fig. 15f) nearly follow the distributions of the associated CHL/TSM, marked by the lowest median values in the GBR region, Tasmania and the North Sea sites ( $0.32$ ,  $0.60$  and  $0.75$  respectively), and higher values ( $> 0.80$ ) in the Cape Verde, Florida, Morocco-W. Md. Sea and Southern California sites. The large variability of CHL/TSM in the North Sea and GBR region (spanning over 3 and 2-orders of magnitude, see Fig. 8) can be related to the high variability in  $a_{\text{phy}}/a_p(440)$  (about 10-fold magnitudes). From Morocco-W. Md. Sea site, the number of  $a_{\text{phy}}/a_p(440)$  data is too low ( $N = 3$ )

compared to the number of CHL/TSM measurements ( $N = 665$ ) yielding a mismatch between both distributions.

The Southern California measurements of  $b_b$  show the highest variability in shapes and amplitudes, with values at 555 nm spanning from 0.0016 to 0.0216  $\text{m}^{-1}$ , encompassing the ranges of  $b_b$  measurements from Acadia and the North Sea sites (Fig. 16a). From the Cape Verde and Morocco-W. Md. Sea sites, only 10  $b_b$  spectra were available, lying at the bottom limit of  $b_b$  measurements from the three previous sites (Fig. 16b).

The distributions of the total backscattering coefficients from Acadia, Cape Verde, Morocco-W. Md. Sea, North Sea and Southern California, and of non-algal particles backscattering coefficients collected at the GBR region and Tasmania sites at 555 nm are presented in Fig. 16c. Quite similar median values of  $b_b(555)$  are observed in Acadia, Southern California and Tasmania coastal waters, being respectively 0.0041, 0.0040 and 0.0034  $\text{m}^{-1}$  (Fig. 16c).

In the GBR region, the coefficient  $b_{\text{bNAP}}(555)$  spans over 3 orders of magnitude around the highest median value 0.021  $\text{m}^{-1}$ . The distributions of  $b_{\text{bNAP}}(555)$  coefficients and TSM (see Fig. 8) differ notably between Tasmania and GBR region.

Lower  $b_b$  values are found in Cape Verde and Morocco-W. Md. Sea sites where only a few backscattering measurements ( $< 10$ ) were available, showing a limited variability.

The total scattering coefficients provided in the North Sea and Gulf of Mexico exhibit high relative variability in the two sites, with the highest amplitudes measured in the Gulf of Mexico (Fig. 16d).

The scattering to backscattering ratio  $b_b/b$  at 555 nm and the mass-specific non-algal particulate backscattering,  $b_{\text{bNAP}}^*$ , at 555 nm were available exclusively from the Tasmanian and GBR coastal waters (Fig. 17a and b). Most of  $b_b/b(555)$  values from the GBR region lie above the percentile 0.75 of  $b_b/b$  measurements in Tasmania, their respective median values being 0.02 and 0.01 (Fig. 17a). Although different distributions are described by  $b_{\text{bNAP}}(555)$  coefficients and TSM from the GBR region and Tasmania sites, the range of  $b_{\text{bNAP}}^*(555)$  observed from the Tasmania site is within that

CoastColour Round  
Robin datasets

B. Nechad et al.

Title Page

Abstract

Instruments

Data Provenance &amp; Structure

Tables

Figures

◀

▶

◀

▶

Back

Close

Full Screen / Esc

Printer-friendly Version

Interactive Discussion



observed from the GBR region (Fig. 17b), which spans from  $5 \times 10^{-4}$  to  $5 \times 10^{-2} \text{ m}^2 \text{ g}^{-1}$ . Generally similar median values are found in the GBR region and Tasmania site, of 0.0053 and  $0.0075 \text{ m}^2 \text{ g}^{-1}$  respectively.

The beam attenuation coefficients were measured in the Gulf of Mexico, covering the spectral range 410 to 710 nm, in the E. Md. Sea at 470, 660 and 670 nm and in Morocco-W. Md. Sea at 660 nm (only coefficients at 660 nm are reported here, Fig. 17c). The coefficients  $c(660)$  span over 3 orders of magnitude, ranging from 0.04 to  $0.9 \text{ m}^{-1}$  in Morocco-W. Md. Sea and the E. Md. Sea (with median values being respectively 0.12 and  $0.46 \text{ m}^{-1}$ ) and from 2 to  $13 \text{ m}^{-1}$  in the Gulf of Mexico (with a median value equal to  $4.91 \text{ m}^{-1}$ ).

### 3.6 Water-leaving radiance reflectance

The match-up field reflectance measurements, the MERIS-RLw (both in the CCRR match-up dataset), and the in situ reflectance spectra (in the CCRR in situ reflectance dataset) are presented successively in Figs. 18–20. Note that the percentage of RLw data per site available from the in situ measurements (i.e. the match-up field and the in situ reflectance datasets) is different from that of the MERIS RLw dataset: 31, 13 and 12 % of the in situ RLw data are provided from the Southern California, Benguela and Indonesian waters respectively, about 8 % from the Chesapeake Bay and Florida sites, and less than 7 % of RLw data were collected at the North Sea site, while 80 % of MERIS RLw measurements came from the North Sea.

The match-up field RLw measurements from the Southern California, Morocco-W. Md. Sea and Benguela sites present the generally lowest amplitudes amongst the CoastColour sites, where more than 75 % of the RLw values at 555 nm,  $\text{RLw}(555)$ , are less than 0.01 and only 6 % of the collected spectra have  $\text{RLw}(555) > 0.02$ . For the Southern California, this is in agreement with the extremely high absorption coefficients reported earlier (see Fig. 14); from Morocco-W. Md. Sea site, the three low match-up field reflectance spectra observed during October 2005 can be associated to the three

Title Page

Abstract

Instruments

Data Provenance & Structure

Tables

Figures

◀

▶

◀

▶

Back

Close

Full Screen / Esc

Printer-friendly Version

Interactive Discussion



**CoastColour Round  
Robin datasets**

B. Nechad et al.

Title Page

Abstract

Instruments

Data Provenance &amp; Structure

Tables

Figures

◀

▶

◀

▶

Back

Close

Full Screen / Esc

Printer-friendly Version

Interactive Discussion



relatively low absorption spectra measured during the same period (Fig. 11), likely to be associated to low TSM concentrations, not represented by the distribution of TSM reported in Fig. 8 (given at different locations and years); for the eutrophic waters of the Benguela site, these low reflectances can be explained by the high phytoplankton absorption and possibly high detrital and/or CDOM absorption. Note that MERIS RLw spectra for the Southern California and Morocco-W. Md. Sea sites show ranges of RLw amplitudes comparable to those of the match-up field spectra.

The MERIS RLw measurements from the E. Md. Sea site show low RLw(555) < 0.01 and higher values at 412 nm ranging from 0.015 to 0.03 and inversely the in situ RLw measurements are slightly higher, up to 0.027, with relatively lower RLw at 412 nm < 0.019. These generally low reflectance values observed by MERIS and in situ are related to the clear oligotrophic waters of the Mediterranean Sea (95 % of Chl *a* data were less than 2 mgm<sup>-3</sup>, with a median value of 0.3 mgm<sup>-3</sup>, Fig. 7). The difference in the spectral shapes between MERIS and in situ measurements can be explained partly by the different periods of observations which were conducted in March 2009 for the in situ data, while only two measurements were available from MERIS in March 2008, all the other measurements were collected during September 2008 and May and October 2005, outside of the blooming period (Barale et al., 2008).

For the Chesapeake Bay, both the 5 MERIS RLw and 81 match-up field RLw spectra exhibit values less than 0.04 at all wavelengths, with 27 % of match-up field RLw(555) higher than 0.02.

From the North Sea site, most of the match-up field (Fig. 18), MERIS RLw (Fig. 19) and in situ spectra (Fig. 20) show a peak around 550–570 nm, not exceeding 0.05, with 50 % of the RLw(555) above 0.02. Lower reflectances are measured at shorter wavelengths (< 450 nm) associated to the higher CDOM and particles absorption in this spectral range (Fig. 12).

The match-up field RLw(555) measurements from the GBR region lie in a range comparable to that observed from the North Sea, but with a significantly different distribution: 86 % of RLw(555) exceeds 0.02. With respect to the North Sea RLw spectra,

CoastColour Round  
Robin datasets

B. Nechad et al.

Title Page

Abstract

Instruments

Data Provenance &amp; Structure

Tables

Figures

◀

▶

◀

▶

Back

Close

Full Screen / Esc

Printer-friendly Version

Interactive Discussion



the spectral shapes and magnitudes of RLw from the GBR region are also markedly different in the blue spectral range. This may be attributed to the notable difference between the spectral shapes and magnitudes of phytoplankton absorption coefficients measured in the North Sea site (Fig. 12) and in the GBR region (Fig. 13) where the concentration of CHL (Chl *a* or TChl *a*) is generally four times lower than in the North Sea (Fig. 7).

Amongst the 47 match-up field reflectance measurements collected at the Gulf of Mexico site, 95 % of RLw around 555 nm were higher than 0.02, 34 % range from 0.03 to 0.05, and one extreme value ( $> 0.15$ ) was measured. The peak of chlorophyll absorption is noticeable around 665 nm on the NOMAD reflectance spectra, which can be related to the generally high Chl *a* measurements (75 % of TChl *a* are higher than  $7.6 \text{ mg m}^{-3}$  and the median value is  $17 \text{ mg m}^{-3}$ , see Fig. 7).

The 127 match-up field reflectance spectra collected from the Indonesian waters exhibit the highest variability of the amplitudes in the red and near-infrared spectra range with some values exceeding 0.1 around 700 nm, likely due to high TSM concentrations as shown in Fig. 8 (TSM may exceed  $100 \text{ g m}^{-3}$ , with a median value about  $25 \text{ g m}^{-3}$ ). At 555 nm, 96 % of the RLw data are above 0.02. Most of the spectra show a minimum around the chlorophyll absorption peak, which can be related to Chl *a* distribution in these waters with a median value about  $7 \text{ mg m}^{-3}$  (Fig. 7).

The 47 Oregon-Washington match-up field spectra exhibit a high variability of reflectance at 412 nm with values ranging from  $3 \times 10^{-3}$  up to  $5 \times 10^{-2}$ , with varying spectral shapes depicting the high spatial and time variability of phytoplankton concentrations noted earlier for that site (Sect. 3.2).

The simulated reflectance spectra in the CCRRv1 dataset are presented in Fig. 21, and related to the ranges of the simulated CHL, MP and  $a_g(443)$  via their colours (as indicated in the key).

The comparison between the CCRRv1 and the IOCCG Algorithm Working Group simulated data (IOCCG, 2006) indicates that the ranges of the total absorption coefficient at 440 nm,  $a(440)$ , and the remote sensing reflectance,  $R_{rs}(440)$  in CCRR are

CoastColour Round  
Robin datasets

B. Nechad et al.

Title Page

Abstract

Instruments

Data Provenance &amp; Structure

Tables

Figures

◀

▶

◀

▶

Back

Close

Full Screen / Esc

Printer-friendly Version

Interactive Discussion



globally within those of IOCCG (Fig. 22a), with a few points of higher total absorption coefficient (maximum in CCRR is  $a(440) = 23.6 \text{ m}^{-1}$ ). While more variability in the reflectance of CCRR for the mid and high ranges of absorption is noted, the ranges of the reflectance band ratios 410 : 440 and 490 : 555 of CCRR are within those of the IOCCG data (Fig. 22b). The large variability of the CCRR reflectance is mainly due to the extended ranges of MP and CHL towards higher concentrations, yielding extended ranges of particle backscattering.

The distribution of reflectance products from the three CCRR datasets is examined through:

- RLw band ratio 490 : 555 vs. RLw band ratio 412 : 443 from reflectance measurements in the match-up field dataset (Fig. 23a) and vs. RLw band ratio 709 : 665 (Fig. 23b). Note that since most of the match-up field measurements contained RLw at 555 nm, that band was chosen instead of MERIS band 560 nm where only few data were available
- RLw band ratio 490 : 560 vs. RLw band ratio 412 : 443 (Fig. 23c) and vs. RLw band ratio 709 : 665 (Fig. 23d) from the MERIS RLw products of the match-up dataset
- RLw band ratio 490 : 560 vs. RLw band ratio 412 : 443 and vs. RLw band ratio 709 : 665 from the in situ reflectance dataset (Fig. 23e and f)

From the match-up field dataset less measurements were available at band 709 nm (only 312 points). There was a general consistency in the distribution of RLw band ratios 709 : 665 (respectively 412 : 443) vs. 490 : 560 from the three datasets except for the in situ reflectances measured in the Benguela waters, which exhibited a high ratio of  $\text{RLw}(412)/\text{RLw}(443) > 1$  in the lower range of reflectance band ratio 490 : 560, likely due to the hypertrophic nature of these waters.

Apart from the extreme ranges of reflectance ratios collected from the Benguela site, the large scatter of points observed in the in situ reflectance dataset from the Gulf

CoastColour Round  
Robin datasets

B. Nechad et al.

Title Page

Abstract

Instruments

Data Provenance &amp; Structure

Tables

Figures

◀

▶

◀

▶

Back

Close

Full Screen / Esc

Printer-friendly Version

Interactive Discussion



of Mexico, the Mediterranean Sea and North Seas (Fig. 23e and f) was drastically reduced in the match-up dataset (that is MERIS RLw) as shown in Fig. 23c and d. The distribution of the ratio  $RLw(709)/RLw(665)$  derived from the simulated dataset reproduced better the ranges covered by the in situ dataset ( $> 70\%$ ) and by the match-up dataset ( $> 95\%$ ), than the distribution of the simulated  $RLw(412)/RLw(443)$ . This is mainly attributable to the fact that the reduced variability of phytoplankton and CDOM inherent optical properties modeled in the simulated dataset does not represent the large natural variability of these IOPs which greatly affect RLw particularly at shorter wavelengths with the effect lessening at longer wavelengths.

### 3.7 Bio-optical relationships

For the comparison of MERIS and the match-up field data, only concurrent data (i.e. within  $\pm 1$  h of MERIS overpass) are considered. Moreover, only match-up field data measured at depths less than 2 m are taken into account since in situ data collected at larger depths are not correlated with the surface remote sensing signal (e.g. in the case of stratified waters).

The number of match-up field TSM and TChl *a* measured above 2 m depth, concurrent with reflectance measurements is 48 and 322 respectively. The number of concurrent in situ IOPs and RLw measurements is low (3 from the North Sea and Morocco-W. Md. Sea sites, 4 from the Acadia and Indonesian waters, 6 from the Gulf of Mexico and 7 from Cape Verde site), except from the Southern California and Florida sites (313 and 66 data respectively). Furthermore, no IOP parameter is available from all these sites (see Table 3b). In the following, the analyses are focused on the distributions of CHL, TSM and reflectance data and their relationships within the match-up, in situ and simulated datasets.

### 3.7.1 CHL vs. RLw

An overview of the optical conditions and CHL ranges covered by the in situ measurements is given by Fig. 24.

Figure 24 presents a scatterplot of CHL vs. RLw band ratio 709 : 665 which shows that the highest CHL concentrations are exhibited during phytoplankton blooms in the Benguela waters where RLw band ratio 709 : 665 is the most sensitive to CHL variations. For  $\text{CHL} < 10 \text{ mg m}^{-3}$ , the measurements from the Oregon-Washington and Benguela sites contain globally lower values of RLw band ratio than in the other sites (left graph in Fig. 24).

The relationship between CHL and reflectance band ratio 490 : 560 is quite consistent throughout the CCRR datasets (Fig. 25), except for the in situ measurements from the Benguela site (blue filled circles in Fig. 25a). This is due to the very high CHL  $> 100 \text{ mg m}^{-3}$  present in the Benguela site -as previously noted in Fig. 24c, but also from the match-up field dataset in Fig. 7b – associated with low RLw ratios outlying the rest of data, and spanning from 0.2 down to 0.02.

### 3.7.2 TSM vs. RLw

Figure 26 shows the distribution of RLw at 620 nm as a function of TSM concentrations, plotted using different colours for each of the CoastColour sites: Indonesian waters, Mediterranean Sea and the North Sea (light and dark green colours are used for the North Sea region to distinguish the Data Provider). Linear regression is applied and the associated equations are reported on the same figure. The slopes of the regression lines range from 0.48 to 0.81. The associated goodness of fit coefficients are 39, 59, 89 and 67% for the Indonesian, North Sea (GKSS), North Sea (RBINS) and Mediterranean Sea measurements respectively. In the GKSS data, most of the scatter occurs at low TSM ranges  $< 7 \text{ g m}^{-3}$ , whereas the measurements from the Indonesian site, taken mainly in highly turbid waters (average and median values being 41.6 and  $26 \text{ g m}^{-3}$  respectively) show a global scatter. This scatter can be due to a high vari-

Title Page

Abstract

Instruments

Data Provenance & Structure

Tables

Figures

◀

▶

◀

▶

Back

Close

Full Screen / Esc

Printer-friendly Version

Interactive Discussion



ability in either the specific inherent optical properties of particles, caused by varying particles size, and/or composition within the sites. The scatter may also be impacted by mismatches of RLw and/or TSM measurements in water with high spatiotemporal variability.

5 The regression line fitting all the data is given by  $\log_{10}(\text{RLw}(620)) = 0.67\log_{10}(\text{TSM}) - 2.82$  (shown by a dashed black line in Fig. 26) with  $R^2 = 69\%$ .

The distribution of the reflectance as a function of TSM concentrations in the three CRR datasets is presented by the scatterplots of TSM vs. the reflectance at 665 nm (Fig. 27a and b) and of TSM vs. the reflectance band ratio 665 : 490 (Fig. 27c and d).  
10 The simulated TSM vs. RLw(665) follow the trend of the match-ups and in situ datasets, with a scatter indicating either variable particulate mass-specific backscattering coefficient different from that assumed in the simulations (Table 11), or measurement errors.

When using the reflectance band ratio, there is a significantly larger scatter of the simulated data due to the effects of CDOM and phytoplankton absorption affecting the reflectance at 490 nm, whereas this scatter is less noticeable in the in situ or match-up data of the 5 regions (Fig. 27c and d) which indicates less variability of CDOM absorption coefficient and phytoplankton concentrations in these measurements than in the modeled dataset.  
15

The general shift between the in situ reflectance dataset and match-up data (Fig. 27 a and b) was not noticeable in the reflectance ratios (Fig. 27c and d), suggesting similar absorption coefficient ratios 665 : 490 in the two datasets, at least in the North Sea regions; at lower TSM range ( $< 10 \text{ g m}^{-3}$ ), the reduced scatter (in the reflectance band ratios vs. TSM, compared to RLw(665) vs. TSM) could also be due to a removal of spectrally white errors.  
20

25 The distributions of the ranges of RLw(665) and RLw(665)/RLw(490) in terms of TSM and within the sites: Indonesian waters, the Mediterranean and the North Seas, is consistent with the distribution of CHL vs. TSM (Fig. 10) in these sites, especially at low TSM  $< 10 \text{ g m}^{-3}$  where CHL is highly correlated with RLw(665).

CoastColour Round Robin datasets

B. Nechad et al.

Title Page

Abstract

Instruments

Data Provenance & Structure

Tables

Figures



Back

Close

Full Screen / Esc

Printer-friendly Version

Interactive Discussion



## 4 Data repository

The match-up, in situ reflectance and simulated datasets are accessible from the PAN-GAEA web site at <http://doi.pangaea.de/10.1594/PANGAEA.841950>. A description of files format and access follows.

The match-up field data for a site “*SiteX*” are stored in the compressed file at [http://hs.pangaea.de/model/ccrr/Matchup\\_Dataset.zip](http://hs.pangaea.de/model/ccrr/Matchup_Dataset.zip), under directory/Match-up\_Dataset/FieldData, in csv files named following the classification of the parameters given in Table 2:

1. *SiteX\_metadata.csv* including the metadata and flags,
2. *SiteX\_biogeochem.csv* including the concentrations of the biogeochemical measurements,
3. *SiteX\_iops.csv* with the inherent optical properties,
4. *SiteX\_aops.csv* which includes the apparent optical properties.

For the North Sea region, two files are provided, having the names “North\_Sea” and “North\_Sea\_Emeco” related to the origin of the data: the North\_Sea\_Emeco data were downloaded from the EMECO website and North\_Sea data from other Data Providers.

MERIS match-up products derived at 5 × 5 pixels box around the locations of the match-up field measurements are provided as csv files, with the headers as listed in Table 7, and stored in the compressed file [http://hs.pangaea.de/model/ccrr/Matchup\\_Dataset.zip](http://hs.pangaea.de/model/ccrr/Matchup_Dataset.zip) under directory/Match-up\_Dataset/MERIS\_5 × 5\_L2R. The MERIS match-up products averaged at each location (from the 5 × 5 pixels box, see Sect. 2.1.2 for details) are stored in csv files, with the headers listed in Table 8, and made available at directory/Match-up\_Dataset/MERIS\_average\_L2R.

The in situ reflectance data are given in one csv file, listing for each Data Provider (in the first column) the sample number, the date, start and end of measurement time, latitude, longitude, the site identification number, the name of the location, the RLw spec-

Title Page

Abstract

Instruments

Data Provenance & Structure

Tables

Figures

◀

▶

◀

▶

Back

Close

Full Screen / Esc

Printer-friendly Version

Interactive Discussion



tra (9 columns for the 9 MERIS selected bands), and CHL and TSM concentrations. These data are stored under the compressed directory InSituReflectance\_Dataset.zip, accessible from the web address [http://hs.pangaea.de/model/ccrr/InSituReflectance\\_Dataset.zip](http://hs.pangaea.de/model/ccrr/InSituReflectance_Dataset.zip).

The simulated data are written in ascii file format, and saved under the directory [http://hs.pangaea.de/model/ccrr/Simulated\\_Dataset.zip](http://hs.pangaea.de/model/ccrr/Simulated_Dataset.zip). The concentrations of CHL, MP and  $a_g(443)$  are given in a separate file (named "Conc.txt") where the simulation numbers going from 1 to 5000 are listed in the first column. Each entry (e.g. each simulation number or line) is associated with a given combination of CHL, MP and  $a_g(443)$ .

The IOPs modelled for each entry, being the total absorption, scattering and backscattering coefficients excluding the pure water contributions, namely  $a_{tot}$ ,  $b_{tot}$ ,  $b_{btot}$ , the absorption by phytoplankton pigments,  $a_{phy}$ , and the ratio of the total backscattering coefficient to the sum of the total absorption and backscattering coefficients  $b_b/(a + b_b)$ , are provided in ascii files called SPC\_Atot.dat, SPC\_Btot.dat, SPC\_BBtot.data, SPC\_Aphy.data and SPC\_BBoABB.dat respectively.

The simulations generated hyperspectral outputs (from 350 to 900 nm, with a 5 nm step), and multispectral outputs at three sensors band centered wavelengths (MODIS-Aqua, MERIS and SeaWiFS), which are specified in the prefix of the output filename SPC = "hyper", "maqua", "meris" or "swifs". The three sun zenith angles ( $x = 0, 40$  and  $60^\circ$ ), assumed successively for the set of the 5000 simulations are given in the output AOPs file names as suffixes "\_szax.dat". Separate files are provided for RLw and Kd, stored as SPC\_RLw\_szax.dat and SPC\_Kd\_szax.dat respectively. The column entry in the spectral data files gives the wavelength (in nm) and the line entry the simulation number.

The simulated data also include also the photosynthetically available radiation  $PAR_{Ed}$  and  $PAR_{Eo}$  defined as the integration over 400 to 700 nm of the spectral downwelling irradiance  $E_d$  and of the scalar irradiance  $E_o$  respectively.  $PAR_{Ed}$  and  $PAR_{Eo}$  were profiled from 0 m above the water surface down to 80 m depth, at 27 depths listed along the

---

**CoastColour Round  
Robin datasets**B. Nechad et al.

---

Title Page

Abstract

Instruments

Data Provenance &amp; Structure

Tables

Figures

◀

▶

◀

▶

Back

Close

Full Screen / Esc

Printer-friendly Version

Interactive Discussion



columns (the line entry is related to the simulation number). The euphotic depths,  $Z_{Eu_{Ed}}$  and  $Z_{Eu_{Eo}}$  defined as the depths where  $PAR_{Ed}$  and  $PAR_{Eo}$  have 1 % of their respective values at the water surface are provided in the files called  $Z_{Eu\_from\_PAR\_Ed\_szax.dat}$  and  $Z_{Eu\_from\_PAR\_Eo\_szax.dat}$  respectively.

The concentrations, IOP and AOP spectral data, PAR and Zeu data files include headers to facilitate reading the data. The IOPs and concentration files are stored under the subfolder “Input IOPs Concentrations” and the simulated RLw, Kd,  $PAR_{Ed}$ ,  $PAR_{Eo}$ ,  $Z_{Eu_{Ed}}$  and  $Z_{Eu_{Eo}}$  under “Output AOPs”.

## 5 Conclusion

The CCRR match-up, in situ and simulated datasets form a large database covering a wide range of water types, from oligotrophic to hypertrophic, and from clear to very turbid waters with a high diversity of IOPs.

The datasets contain 336 in situ reflectance spectra (covering the spectral range 412 to 709 nm) from five CoastColour sites, 957 match-up field reflectance spectra from 13 sites and 457 MERIS RLw spectra from 11 sites which show global consistency over the match-up sites, despite the absence of harmonized protocols used for RLw measurements by the different laboratories. 80 % of the MERIS RLw measurements were provided from the North Sea, matching various in situ water quality parameters collected at this site. This is balanced by the distribution of RLw measurements, throughout the CoastColour sites, given in the match-up field and in situ reflectance datasets where less than 5 % of RLw spectra were available from the North Sea, while 23 % of the match-up field IOP data (excluding turbidity) were provided for that site.

The high quality reflectance datasets along with the biogeochemical (CHL, TSM) and inherent optical properties provided at 17 CoastColour sites, covering the period 2005 to 2010, were fully documented and made available publicly for use in ocean colour algorithm testing.

Title Page

Abstract

Instruments

Data Provenance & Structure

Tables

Figures

⏪

⏩

◀

▶

Back

Close

Full Screen / Esc

Printer-friendly Version

Interactive Discussion



**CoastColour Round  
Robin datasets**

B. Nechad et al.

[Title Page](#)[Abstract](#)[Instruments](#)[Data Provenance & Structure](#)[Tables](#)[Figures](#)[⏪](#)[⏩](#)[◀](#)[▶](#)[Back](#)[Close](#)[Full Screen / Esc](#)[Printer-friendly Version](#)[Interactive Discussion](#)

The simulated dataset includes 5000 reflectance spectra and the associated concentrations and inherent optical properties of chlorophyll *a*, mineral particles and CDOM. The simulated reflectance data have been compared to the in situ and match-up reflectance data, showing a global consistency and giving clues for the discrepancies noticed (e.g. variable inherent optical properties, measurement uncertainties).

The strengths and weaknesses of each individual dataset are recognized, e.g. an in situ measurement represents “sea truth” better than simulated data, but is subject to measurement uncertainty and represents only a small volume. Testing of an algorithm on all three datasets using respectively MERIS, in situ and simulated RLW input, has significantly added value: evaluating the robustness of an ocean colour algorithm against remote-sensing measurements uncertainties, identifying its domain of validity (e.g. the detection or saturation limits) and testing its performance on various regions, days and daytimes, sea and sky conditions. . . etc. Such exercises may point out the disadvantage/advantage to use an algorithm for a regional or global application.

Oceanographic databases have been built during the last few years and made available to the scientific community (e.g. open ocean phytoplankton data by O’Brien et al., 2012 and Buitenhuis et al., 2013) which facilitates the sharing of data and stimulates collaboration between the research institutes. In this paper, the first public optical/biogeochemical database was established representing the core of an open resource dedicated to Case 2 remote sensing data validation and algorithm testing. With joint efforts from the research centers and laboratories, this database may be updated with extended in situ data for the existing sites and for new regions in coastal and inland waters, with extra information (e.g. data quality flags), and with artificial datasets covering extra ranges of optical properties (e.g. extremely absorbing waters, extremely turbid waters), and/or underlying new bio-optical models.

*Acknowledgements.* This work is part of the CoastColour project, funded by the European Space Agency. The CSIRO measurements were funded by the CSIRO Wealth from Oceans Flagship.

We thank the in situ Data Providers:

– Curtiss O. Davis, Ricardo M. Letelier, Angelique E. White and Marnie Jo Zirbel for collecting and processing the CEOAS dataset

– Hayley Evers-King, Mark Matthews and Lisl Robertson for processing the CSIR dataset.

– Roland Doerffer, Wolfgang Schoenfeld and Friedhelm Schroeder for providing the GKSS dataset

– Rodney Forster for providing the Cefas Chl *a* dataset, included in the EMECO dataset

– Aristomenis P. Karageorgis, Kalliopi A. Pagou, Dimitris Tsoiakos and Christina Zeri for collecting and processing the HCMR dataset. The data from HCMR was acquired in the framework of SESAME

– EC FP6 Integrated Project: Southern European Seas: Assessing and Modeling Ecosystem changes; HERMES

– EC FP6 Integrated Project: Hotspot Ecosystem Research on the Margins of European Seas; and SARONIKOS: Monitoring of the inner Saronikos Gulf ecosystems, under the influence of the Psittalia sewage treatment plant. Ministry of Environment of the Hellenic Government.

– Yu-Hwan Ahn and YoungJe Park for providing the KORDI dataset

– Syarif Budhiman for processing the ITC dataset

– Guy Westbrook for providing the MII dataset

– Bryan A. Franz for processing the NOMAD dataset

– Francis Gohin for the Ifremer dataset

– Zhongping Lee (now at the University of Massachusetts Boston) for providing the MSU dataset

– Griet Neukermans for collecting and processing the RBINS dataset

– Xabier Guinda, Beatriz Echavarri, Isabel Santamaría and Pablo Ruíz for the UNICAN data collection and processing

– Elisabete Mota (formerly in the Center of Oceanography, FCUL) and Katharina Poser (formerly in Brockman Consult) are thanked for their participation in the collection and organization of the in situ datasets.

## ESSDD

8, 173–258, 2015

### CoastColour Round Robin datasets

B. Nechad et al.

Title Page

Abstract

Instruments

Data Provenance & Structure

Tables

Figures



Back

Close

Full Screen / Esc

Printer-friendly Version

Interactive Discussion



## References

- Albert, A. and Mobley, C. D.: An analytical model for subsurface irradiance and remote sensing reflectance in deep and shallow Case 2 waters, *Opt. Express*, 11, 2873–2890, 2003.
- Arar, E. J. and Collins, G. B.: In vitro determination of chlorophyll *a* and pheophytin *a* in marine and freshwater algae by fluorescence, method 445.0. National Exposure Research Laboratory, US Environmental Protection Agency, Cincinnati, OH, USA, 1992.
- Babin, M., Morel, A., Fournier-Sicre, V., Fell, F., and Stramski, D.: Light scattering properties of marine particles in coastal and open ocean waters as related to the particle mass concentration, *Limnol. Oceanogr.*, 28, 843–859, 2003a.
- Babin, M., Stramski, D., Ferrari, G. M., Claustre, H., Bricaud, A., Obolensky, G., and Hoepffner, N.: Variations in the light absorption coefficients of phytoplankton, nonalgal particles and dissolved organic matter in coastal waters around Europe, *J. Geophys. Res.*, 108, 3211, doi:10.1029/2001JC000882, 2003b.
- Barale, V., Jaquet, J.-M., and Ndiayé, M.: Algal blooming patterns and anomalies in the Mediterranean Sea as derived from the SeaWiFS data set (1998–2003), *Remote Sens. Environ.*, 112, 3300–3313, 2008.
- Barlow, R. G., Cummings, D. G., and Gibb, S. W.: Improved resolution of mono and divinyl chlorophylls *a* and *b* and zeaxanthin and lutein in phytoplankton extracts using reverse phase C-8 HPLC, *Mar. Ecol.-Prog. Ser.*, 161, 303–307, 1997.
- Blondeau-Patissier, D., Brando, V. E., Oubelkheir, K., Dekker, A. G., Clementson, L. A., and Daniel, P.: Bio-optical variability of the absorption and scattering properties of the Queensland inshore and reef waters, Australia, *J. Geophys. Res.*, 114, C5, doi:10.1029/2008JC005039, 2009.
- Bouvet, M. and Ramoino, F.: Equalization of MERIS L1b products from the 2nd reprocessing, Technical Report, European Space Agency TN TEC-EEP/2009.251/MB, ESA, 2010.
- Brewin, R. J. W., Sathyendranath, S., Müller, D., Brockmann, C., Deschamps, P.-Y., Devred, E., Doerffer, R., Fomferra, N., Franz, B., Grant, M., Groom, S., Horseman, A., Hu, C., Krasemann, H., Lee, Z.-P., Maritorena, S., Mélin, F., Peters, M., Platt, T., Regner, P., Smyth, T., Steinmetz, F., Swinton, J., Werdell, J., and White III, G. N.: The Ocean Colour Climate Initiative: III. A round-robin comparison on in-water bio-optical algorithms, *Remote Sens. Environ.*, 30, doi:10.1016/j.rse.2013.09.016, 2013.

## CoastColour Round Robin datasets

B. Nechad et al.

Title Page

Abstract

Instruments

Data Provenance & Structure

Tables

Figures



Back

Close

Full Screen / Esc

Printer-friendly Version

Interactive Discussion



CoastColour Round  
Robin datasets

B. Nechad et al.

Title Page

Abstract

Instruments

Data Provenance &amp; Structure

Tables

Figures

◀

▶

◀

▶

Back

Close

Full Screen / Esc

Printer-friendly Version

Interactive Discussion



- Bricaud, A., Morel, A., Babin, M., Allali, K., and Claustre, H.: Variations of light absorption by suspended particles with chlorophyll *a* concentration in oceanic (Case 1) waters: analysis and implications for bio-optical models, *J. Geophys. Res.*, 103, 31033–31044, 1998.
- 5 Brodie, J., De'ath, G., Devlin, M., Furnas, M. J., and Wright, M.: Spatial and temporal patterns of near surface chlorophyll *a* in the Great Barrier Reef lagoon, *Mar. Freshwater Res.*, 58, 342–353, 2007.
- Buitenhuis, E. T., Vogt, M., Moriarty, R., Bednaršek, N., Doney, S. C., Leblanc, K., Le Quéré, C., Luo, Y.-W., O'Brien, C., O'Brien, T., Peloquin, J., Schiebel, R., and Swan, C.: MAREDAT: towards a world atlas of MARine Ecosystem DATA, *Earth Syst. Sci. Data*, 5, 227–239, doi:10.5194/essd-5-227-2013, 2013.
- 10 Caballero, I., Morris, E. P., Prieto, L., and Navarro, G.: The influence of the Guadalquivir River on the spatio-temporal variability of suspended solids and chlorophyll in the Eastern Gulf of Cadiz, *Mediterranean Marine Science*, 15, 721–738, 2014.
- Chavez, F. P., Pennington, J. T., Castro, C. G., Ryan, J. P., Michisaki, R. P., Schlining, B., Walz, P., Buck, K. R., McFadyen, A., and Collins, C. A.: Biological and chemical consequences of the 1997–1998 El Niño in central California waters, *Prog. Oceanogr.*, 54, 205–232, 2002.
- 15 Cherukuru, N., Brando, V. E., Schroeder, T., Clementson, L. A., and Dekker, A. G.: Influence of river discharge and ocean currents on coastal optical properties, *Cont. Shelf Res.*, 84, 188–203, 2014.
- Clesceri, L. S., Greenberg, A. E., and Eaton, A. D.: Standard methods for the examination of water and wastewater, 20th edn., American Public Health Association, Washington D.C., USA, 1325 pp., 1998.
- Doerffer, R.: Protocols for the Validation of MERIS Water Products, European Space Agency, ESRIN, Frascati, Italy, Doc. no. PO-TN-MEL-GS-0043, p. 1–42, Issue 1, Revision 3, 25 January 2002.
- Doerffer, R.: Alternative Atmospheric Correction Procedure for Case 2 Water Remote Sensing using MERIS, Algorithm Theoretical Basis Document (ATBD) 2.255, version 1.0, Helmholtz-Zentrum Geesthacht, 21502, Germany, 2011.
- 30 Doerffer, R. and Schönfeld, W.: Validation transect between Cuxhaven and Helgoland, GKSS Technical Note (18 February 2009), Helmholtz-Zentrum Geesthacht, 21502, Germany, 2009.

## CoastColour Round Robin datasets

B. Nechad et al.

Title Page

Abstract

Instruments

Data Provenance &amp; Structure

Tables

Figures

◀

▶

◀

▶

Back

Close

Full Screen / Esc

Printer-friendly Version

Interactive Discussion



- Dolan, J. R., Claustre, H., Carlotti, F., Plounevez, S., and Moutin, T.: Microzooplankton diversity: relationships of tintinnid ciliates with resources, competitors and predators from the Atlantic Coast of Morocco to the Eastern Mediterranean, *Deep-Sea Res. Pt. I*, 49, 1217–1232, 2002.
- 5 Franz, B. A. and Werdell, P. J.: A generalized framework for modeling of Inherent Optical Properties in ocean remote sensing applications, *Proceedings of Ocean Optics XX*, Anchorage, Alaska, USA, 27 September–1 October 2010.
- Freudenthal, T., Meggers, H., Henderiks, J., Kuhlmann, H., Moreno, A., and Wefer, G.: Upwelling intensity and filament activity off Morocco during the last 250,000 years, *Deep-Sea Res. Pt. II*, 49, 3655–3674, 2002.
- 10 Groom, S. B., Herut, B., Brenner, S., Zodiatis, G., Psarra, S., Kress, N., Krom, M. D., Law, C. S., and Dracopoulos, P.: Satellite-derived spatial and temporal biological variability in the Cyprus Eddy, *Deep-Sea Res. Pt. II*, 52, 2990–3010, 2005.
- Groom, S. B., Martinez-Vicente, V., Fishwick, J. R., Tilstone, G., Moore, G., Smyth, T. J., and Harbour, D.: The Western English Channel observatory: optical characteristics of station 4, *J. Marine Syst.*, 77, 278–295, 2009.
- 15 Harrison, A. W. and Coombes, C. A.: An opaque cloud cover model of sky short wavelength radiance, *Sol. Energy*, 41, 387–392, 1988.
- Holm-Hansen, O., Lorenzen, C. J., Holmes, R. W., and Strickland, J. D. H.: Fluorometric determination of chlorophyll, *Journal du Conseil*, 30, 3–15, 1965.
- 20 Hooker, S. B., Van Heukelem, L., Thomas, C. S., Claustre, H., Ras, J., Barlow, R. G., Sessions, H., Schlüter, L., Perl, J., Trees, C. C., Stuart, V., Head, E., Clementson, L. A., Fishwick, J. R., Llewellyn, C., and Aiken, J.: The Second SeaWiFS HPLC Analysis Round-Robin Experiment (SeaHARRE-2), NASA Aeronautics and Space Information, Goddard Space Flight Center, Greenbelt, Maryland, 2005.
- 25 IOC/UNESCO: Protocols for Joint Global Ocean Carbon Flux Study (JGOFS) Core Measurements, JGOFS Report No. 19 (Reprint of the IOC Manuals and Guides No. 29, UNESCO, Paris, 1994), 170 pp., 1996.
- Karageorgis, A. P., Georgopoulos, D., Kanellopoulos, T. D., Mikkelsen, O. A., Pagou, K., Kontoyiannis, H., Pavlidou, A., and Anagnostou, C.: Spatial and seasonal variability of particulate matter optical and size properties in the Eastern Mediterranean Sea, *J. Marine Syst.*, 105–108, 123–134, 2012.
- 30

**CoastColour Round  
Robin datasets**

B. Nechad et al.

[Title Page](#)[Abstract](#)[Instruments](#)[Data Provenance & Structure](#)[Tables](#)[Figures](#)[Back](#)[Close](#)[Full Screen / Esc](#)[Printer-friendly Version](#)[Interactive Discussion](#)

- Llewellyn, C. A., Fishwick, J. R., and Blackford, J. C.: Phytoplankton community assemblage in the English Channel: a comparison using chlorophyll *a* derived from HPLC-CHEMTAX and carbon derived from microscopy cell counts, *J. Plankton Res.*, 27, 103–119, 2005.
- Loisel, H. and Morel, A.: Light scattering and chlorophyll concentration in Case 1 waters: a re-examination, *Limnol. Oceanogr.-Meth.*, 43, 847–857, 1998.
- Loisel, H., Vantrepotte, V., Norkvist, K., Mériaux, X., Kheireddine, M., Ras, J., Pujo-Pay, M., Combet, Y., Leblanc, K., Dall’Olmo, G., Mauriac, R., Dessailly, D., and Moutin, T.: Characterization of the bio-optical anomaly and diurnal variability of particulate matter, as seen from scattering and backscattering coefficients, in ultra-oligotrophic eddies of the Mediterranean Sea, *Biogeosciences*, 8, 3295–3317, doi:10.5194/bg-8-3295-2011, 2011.
- Maritorena, S., Lee, Z.-P., Du, K.-P., Loisel, H., Doerffer, R., Roesler, C., Tanaka, A., Babin, M., and Kopelevich, O. V.: Synthetic and in situ data sets for algorithm testing. *Remote Sensing of Inherent Optical Properties: Fundamentals, Tests of Algorithms, and Applications*, IOCCG., Dartmouth, Canada, 73–79, 20065, 13–18, 2006.
- Martinez-Vicente, V., Land, P. E., Tilstone, G. H., Widdicombe, C., and Fishwick, J. R.: Particulate scattering and backscattering related to water constituents and seasonal changes in the Western English Channel, *J. Plankton Res.*, 32, 603–619, 2010.
- Mobley, C. D.: *Light and Water: Radiative Transfer in Natural Waters*, Academic Press, London, 1994.
- Mobley, C. D.: Estimation of the remote sensing reflectance from above-surface measurements, *Appl. Optics*, 38, 7442–7455, 1999.
- Mobley, C. D. and Sundman, L. K.: *HYDROLIGHT 5/ECOLIGHT 5 Technical Documentation*, Sequoia Scientific, Incorporated, Bellevue, WA, 98005, 95, 2008.
- Morel, A. and Prieur, L.: Analysis of variations in ocean color, *Limnol. Oceanogr.*, 22, 709–722, 1977.
- Morel, A., Antoine, D., and Gentili, B.: Bidirectional reflectance of oceanic waters: accounting for Raman emission and varying particle scattering phase function, *Appl. Optics*, 41, 6289–6306, 2002.
- O’Brien, C. J., Peloquin, J. A., Vogt, M., Heinle, M., Gruber, N., Ajani, P., Andruleit, H., Arístegui, J., Beaufort, L., Estrada, M., Karentz, D., Koczyńska, E., Lee, R., Poulton, A. J., Pritchard, T., and Widdicombe, C.: Global marine plankton functional type biomass distributions: coccolithophores, *Earth Syst. Sci. Data*, 5, 259–276, doi:10.5194/essd-5-259-2013, 2013.

## CoastColour Round Robin datasets

B. Nechad et al.

Title Page

Abstract

Instruments

Data Provenance &amp; Structure

Tables

Figures



Back

Close

Full Screen / Esc

Printer-friendly Version

Interactive Discussion



- O'Reilly, J. E., Maritorena, S., Mitchell, B. G., Siegel, D. A., Carder, K. L., Garver, S. A., Kahru, M., and McClain, C. R.: Ocean color chlorophyll algorithms for SeaWiFS, *J. Geophys. Res.*, 103, 24937–24953, 1998.
- Odermatt, D., Gitelson, A. A., Brando, V. E., and Schaepman, M.: Review of constituent retrieval in optically deep and complex waters from satellite imagery, *Remote Sens. Environ.*, 118, 116–126, 2012.
- Oubelkheir, K., Claustre, H., Sciandra, A., and Babin, M.: Bio-optical and biogeochemical properties of different trophic regimes in oceanic waters, *Limnol. Oceanogr.*, 50, 1795–1809, 2005.
- Oubelkheir, K., Clementson, L. A., Webster, I., Ford, P., Dekker, A. G., Radke, L., and Daniel, P.: Using inherent optical properties to investigate biogeochemical dynamics in a tropical macrotidal coastal system, *J. Geophys. Res. Oceans*, 111, C7, doi:10.1029/2005JC003113, 2006.
- Parsons, T. R., Maita, Y., and Lalli, C. M.: *A Manual of Chemical and Biological Methods for Seawater Analysis*, Pergamon Press, New York, 173 pp., 1984.
- Pegau, W. S., Zaneveld, J. R. V., Mitchell, B. G., Mueller, J. L., Kahru, M., Wieland, J., and Stramska, M.: *Inherent Optical Properties: Instruments, Characterizations, Field Measurements and Data Analysis Protocols*, Ocean optics for satellite ocean color sensor validation. NASA Tech Memo, 211621 Greenbelt, 76 pp., 2003.
- Pitcher, G. C. and Probyn, T. A.: Anoxia in southern Benguela during the autumn of 2009 and its linkage to a bloom of the dinoflagellate *Ceratium balechii*, *Harmful Algae*, 11, 23–32, 2011.
- Prieto, L., Navarro, G., Rodríguez-Gálvez, S., Huertas, I. E., Naranjo, J. M., and Ruiz, J.: Oceanographic and meteorological forcing the pelagic ecosystem on the Gulf of Cadiz shelf (SW Iberian Peninsula), *Cont. Shelf Res.*, 29, 2122–2137, 2009.
- Probyn, T. A.: Nitrogen uptake by size-fractionated phytoplankton populations in the southern Benguela upwelling system, *Mar. Ecol.-Prog. Ser.*, 22, 249–258, 1985.
- Ruddick, K., Brockmann, C., Doerffer, R., Lee, Z., Brotas, V., Fomferra, N., Groom, S., Krasemann, H., Martinez-Vicente, V., Sá, C., Santer, R., Sathyendranath, S., Stelzer, K., and Pinnock, S.: The CoastColour project regional algorithm round robin exercise, *SPIE Proceedings Vol. 7858, Remote Sensing of the Coastal Ocean, Land, and Atmosphere Environment*, 785807, doi:10.1117/12.869506, 4 November 2010.

## CoastColour Round Robin datasets

B. Nechad et al.

Title Page

Abstract

Instruments

Data Provenance & Structure

Tables

Figures

◀

▶

◀

▶

Back

Close

Full Screen / Esc

Printer-friendly Version

Interactive Discussion



Ruddick, K. G., De Cauwer, V., Park, Y., and Moore, G.: Seaborne measurements of near infrared water-leaving reflectance – the similarity spectrum for turbid waters, *Limnol. Oceanogr.*, 51, 1167–1179, 2006.

Schaffelke, B., Carleton, J., Skuza, M., Zagorskis, I., and Furnas, M. J.: Water quality in the inshore Great Barrier Reef lagoon: implications for long-term monitoring and management, *Mar. Pollut. Bull.*, 65, 249–260, 2012.

Tassan, S. and Ferrari, G. M.: An alternative approach to absorption measurements of aquatic particles retained on filters, *Limnol. Oceanogr.*, 40, 1358–1368, 1995.

Tilstone, G., Moore, G., Sorensen, K., Doerffer, R., Rottgers, R., Ruddick, K. G., Pasterkamp, R., and Jorgensen, P. V.: REVAMP Regional Validation of MERIS Chlorophyll products in North Sea coastal waters: Protocols document, Proceedings of MERIS and AATSR Calibration and Geophysical Validation (MAVT-2003), Frascati: European Space Agency Publication WPP-233, 2002.

Tilstone, G., Peters, S., van Der Woerd, H., Eleveld, M., Ruddick, K., Schönfeld, W., Krusemann, H., Martinez-Vicente, V., Blondeau-Patissier, D., Jorgensen, P. V., Rottgers, R., and Sorensen, K.: Variability in specific-absorption properties and their use in Ocean Colour Algorithms for MERIS in North Sea coastal waters, *Remote Sens. Environ.*, 118, 320–338, 2012.

Tzortziou, M., Subramaniam, A., Herman, J. R., Gallegos, C. L., Neale, P. J., and Harding, L. W. J.: Remote sensing reflectance and inherent optical properties in the mid Chesapeake Bay, *Estuar. Coast. Shelf S.*, 72, 16–32, 2007.

van der Linde, D. W.: Protocol for the determination of total suspended matter in oceans and coastal zones, Technical Note I.98.182, Joint Research Centre, Ispra, 1998.

Van Heukelem, L. and Thomas, C. S.: Computer-assisted high-performance liquid chromatography method development with applications to the isolation and analysis of phytoplankton pigments, *J. Chromatogr. A*, 910, 31–49, 2001.

Werdell, P. J.: An evaluation of Inherent Optical Property data for inclusion in the NASA bio-Optical Marine Algorithm Data set, NASA Ocean Biology Processing Group, Science Systems and Applications, Inc., NASA Goddard Space Flight Center, Greenbelt, Md., 2005.

Werdell, P. J. and Bailey, S. W.: An improved in situ bio-optical data set for ocean color algorithm development and satellite data product validation, *Remote Sens. Environ.*, 98, 122–140, 2005.

Werdell, P. J., Bailey, S. W., Fargion, G. S., Pietras, K., Knobelspiesse, K. D., Feldman, G. C., and McClain, C.: Unique data repository facilitates ocean color satellite validation, EOS T. Am. Geophys. Un., 84, 377–392, 2003.

5 Werdell, P. J., Franz, B. A., Bailey, S. W., Feldman, G. C., Boss, E., Brando, V. E., Dowell, M. D., Hirata, T., Lavender, S. J., Lee, Z., Loisel, H., Maritorena, S., Mélin, F., Moore, T. S., Smyth, T. J., Antoine, D., Devred, E., Hembise Fanton d'Andon, O., and Mangin, A.: Generalized ocean color inversion model for retrieving marine inherent optical properties, Appl. Optics, 52, 2019–2037, 2013.

10 Wright, S. W., Jeffrey, S. W., Mantoura, R. F. C., Llewellyn, C. A., Bjornland, T., and Repeta, D. J.: Improved HPLC method for the analysis of chlorophylls and carotenoids from marine phytoplankton, Mar. Ecol.-Prog. Ser., 77, 183–196, 1991.

## ESSDD

8, 173–258, 2015

### CoastColour Round Robin datasets

B. Nechad et al.

Title Page

Abstract

Instruments

Data Provenance & Structure

Tables

Figures

◀

▶

◀

▶

Back

Close

Full Screen / Esc

Printer-friendly Version

Interactive Discussion



**Table 1.** Acronyms of in situ data sources, and associated websites where the original data and methodologies are available.

Acronym	Name
CEOAS/OSU (CEOAS)	College of Earth, Ocean and Atmospheric Sciences – Oregon State university (USA)
CSIC	Spanish Institute for Marine Sciences (Spain)
CSIR	Council for Scientific and Industrial Research (South Africa)
CSIRO	Commonwealth Scientific and Industrial Research Organisation (Australia)
EMECO	European Marine ECosystem Observatory <a href="http://www.emecodata.net">http://www.emecodata.net</a>
GKSS	Centre for Materials and Coastal Research, Helmholtz-Zentrum Geesthacht (Germany)
HCMR	Hellenic Centre for Marine Research (Greece)
Ifremer	French Research Institute for Exploration of the Sea (France) <a href="http://wwz.ifremer.fr/lerpc/Activites-et-Missions/Surveillance/REPHY">http://wwz.ifremer.fr/lerpc/Activites-et-Missions/Surveillance/REPHY</a>
ITC	International Institute for Geo-Information Science and Earth Observation (Netherlands)
KORDI	Korea Ocean Research and Development Institute (Korea)
MII	Marine Institute of Ireland (Ireland) <a href="http://data.marine.ie">http://data.marine.ie</a>
MSU	Mississippi State University (USA)
NOAA	National Oceanic and Atmospheric Administration (USA)
NOMAD	NASA bio-optical Marine Algorithm Data set. <a href="http://seabass.gsfc.nasa.gov">http://seabass.gsfc.nasa.gov</a>
PML	Plymouth Marine Laboratory (UK)
RBINS	Royal Belgian Institute for Natural Sciences (Belgium)
UCSB	University of California at Santa Barbara, Earth Research Institute (USA)
UNICAN	Environmental Hydraulics Institute of the University of Cantabria (Spain)

**CoastColour Round Robin datasets**

B. Nechad et al.

Title Page

Abstract

Instruments

Data Provenance & Structure

Tables

Figures



Back

Close

Full Screen / Esc

Printer-friendly Version

Interactive Discussion



CoastColour Round Robin datasets

B. Nechad et al.

Title Page

Abstract Instruments

Data Provenance & Structure

Tables Figures

◀ ▶

◀ ▶

Back Close

Full Screen / Esc

Printer-friendly Version

Interactive Discussion



**Table 2.** Metadata, IOPs and AOPs given at wavelength  $\lambda$ , and biogeochemical in situ measurements available for the CoastColour sites. The two notations Chl *a* and TChl *a* refer to Chlorophyll *a* concentration measured by High-Performance Liquid Chromatography (HPLC) and by fluorometry respectively.

Metadata	Notation	Units	Concentrations	Notation	Units
Date, Time		–	Chlorophyll <i>a</i> (fluorometry)	Chl <i>a</i>	mg m <sup>-3</sup>
Station, Cruise		–	Total chlorophyll <i>a</i> (HPLC)	TChl <i>a</i>	mg m <sup>-3</sup>
File name, File_id (station)		–	TSM	TSM	g m <sup>-3</sup>
Latitude, longitude		degree	Non algal particulate matter	NAP	g m <sup>-3</sup>
Wind speed		m s <sup>-1</sup>	Particulate inorganic matter	PIM	g m <sup>-3</sup>
Cloud cover		–	Particulate organic matter	POM	g m <sup>-3</sup>
Measurement depth		m	CDOM fluorescence	CDOMf	Qse
Secchi depth		m			
Water depth		m	Flags	Notation	Units
Photoc depth	$Z_{p\%}$	m	General flag	Flag	–
Mixed layer depth	MLD	m	Location flag	Location_flag	–
Temperature		°C	Time flag	Time_flag	–
Salinity		psu	Chlorophyll <i>a</i> method	Chla_flag	–
Provider		–	CoastColour Product	CCP_flag	–
IOPs	Notation	Units	AOPs	Notation	Units
Total absorption coefficient	$a(\lambda)$	m <sup>-1</sup>	Remote-sensing reflectance	Rrs ( $\lambda$ )	sr <sup>-1</sup>
Particles absorption coefficient	$a_p(\lambda)$	m <sup>-1</sup>	Water-leaving reflectance	RLw ( $\lambda$ )	–
NAP absorption coefficient	$a_{NAP}(\lambda)$	m <sup>-1</sup>	Water-leaving radiance (or above-water upwelling	Lw ( $\lambda$ )	mW cm <sup>-2</sup>
Absorption by phytoplankton	$a_{ph}(\lambda)$	m <sup>-1</sup>	radiance)		$\mu\text{m}^{-1} \text{sr}^{-1}$
Absorption by detritus	$a_d(\lambda)$	m <sup>-1</sup>	Above-water downwelling irradiance (or incident irradiance)	Es ( $\lambda$ )	mW cm <sup>-2</sup>
CDOM absorption coefficient	$a_g(\lambda)$	m <sup>-1</sup>	Downwelling irradiance	Ed ( $\lambda$ )	mW cm <sup>-2</sup>
Total (back)scattering coefficient	$b_{(b)}(\lambda)$	m <sup>-1</sup>			$\mu\text{m}^{-1}$
NAP scattering coefficient	$b_{NAP}(\lambda)$	m <sup>-1</sup>	Diffuse attenuation of Ed	Kd ( $\lambda$ )	m <sup>-1</sup>
NAP backscattering coefficient	$b_{bNAP}(\lambda)$	m <sup>-1</sup>	Diffuse attenuation of PAR	$K_{par}$	m <sup>-1</sup>
Backscattering ratio	$b_{bp}(\lambda)/b_p(\lambda)$	–			
Total beam attenuation coefficient	$c(\lambda)$	m <sup>-1</sup>			
Particles beam attenuation coefficient	$c_p(\lambda)$	m <sup>-1</sup>			
Turbidity		FNU, FTU			



CoastColour Round Robin datasets

B. Nechad et al.

Title Page

Abstract Instruments

Data Provenance & Structure

Tables Figures

◀ ▶

◀ ▶

Back Close

Full Screen / Esc

Printer-friendly Version

Interactive Discussion



Table 3b. Number of IOP and AOP match-up field measurements.

WQ	Coast- Colour site	Acadia	Benguela	Cape Verde	Central California	Chesapeake Bay	E. Md. Sea	East China Sea	Florida	GBR region	Gulf of Mexico	Indonesian waters	Morocco-W. Md. Sea	North Sea	Oregon- Washington	Southern California	Tasmania	Trinidad and Tobago	Total
<i>a</i>									63	63	6			117		342	19		610
<i>a<sub>p</sub></i>				7					66	63			3	188		346	21		694
<i>a<sub>phy</sub></i>				7					66	63			3	176		346	21		682
<i>a<sub>NAP</sub></i> , <i>a<sub>NAP</sub></i>										63							21		84
<i>a<sub>d</sub></i>				7					66				3	188		347			611
<i>a<sub>g</sub></i>		4							65	63		4		129		342	19		626
<i>b</i>											6			54					60
<i>b<sub>b</sub></i>		23		7									3	28		269			330
<i>b<sub>b</sub>/b</i>										63								21	84
<i>b<sub>NAP</sub></i> , <i>b<sub>NAP</sub></i>										25									25
<i>b<sub>bNAP</sub></i> , <i>b<sub>bNAP</sub></i>										63									84
<i>c</i>							139				6		6	116					267
<i>c<sub>p</sub></i>							34												34
Turbidity													30	2157					2187
CDOMf							132												132
Kd		42		8		69		4				8	3	6		16		11	167
RLw		76	84	8		81		85	15	47		127	3	54	47	319		11	957
kpar		38		5		35						8	3	4		15		10	118
<i>Z</i> <sub>37%</sub>		42		8		69						8	3	5		16		10	161
<i>Z</i> <sub>10%</sub>		42		8		66						8	3	6		15		10	158
<i>Z</i> <sub>1%</sub>		41		8		61						8	3	6		11		10	148

**Table 4.** Instrument and methods of chlorophyll *a* measurement in the CCRR match-up dataset.

Data provider	Instrument	Filters, diameter (mm), nominal pore size ( $\mu\text{m}$ )	TCHL-a measurement Method (HPLC)	Chl <i>a</i> measurement Method
CEOAS		Whatman GF/F, N/A, 0.7	HPLC	–
CSIC	Turner Model 10	Whatman GF/F, N/A, 0.7	–	JGOFS protocols (IOC/UNESCO, 1996)
CSIR	Turner Model 10-AU		–	(Parsons et al., 1984)
CSIRO		GF/F, 47, 0.7	(Wright et al., 1991), (Van Heukelem and Thomas, 2001)	–
EMECO	5 LEDs (Ferrybox)		–	In vivo Fluorometry
GKSS			(Doerffer and Schönfeld, 2009)	–
HCMR	Turner Model10-AU Turner TD700	Nucleopore of Millipore, membrane polycarbonate, 47, 0.2	–	EPA Method 445 (Holm-Hansen et al., 1965) adapted by (Arar and Collins, 1992)
Ifremer	Turner C7, C3	–	–	Fluorometry
IOW				Fluorometry
ITC		Membrane filter, 47, 0.45	–	Spectrophotometry (Clesceri et al., 1998)
NOAA				Fluorometry
NOMAD	Various (see references)		(Hooker et al., 2005)	(Werdell and Bailey, 2005), (Pegau et al., 2003)
PML	Hypersil 3 mm C8 Thermo-separations <sup>®</sup> and Agilent <sup>®</sup>		(Barlow et al., 1997; Lewellyn et al., 2005)	–
UCSB	Turner Model 10-AU		(Van Heukelem and Thomas, 2001)	(Mueller et al., 2003)
UNICAN	Hach Lange DR-5000		–	Spectrophotometry

Title Page

Abstract

Instruments

Data Provenance &amp; Structure

Tables

Figures

I ◀

▶ I

◀

▶

Back

Close

Full Screen / Esc

Printer-friendly Version

Interactive Discussion



CoastColour Round  
Robin datasets

B. Nechad et al.

Title Page

Abstract

Instruments

Data Provenance &amp; Structure

Tables

Figures

◀

▶

◀

▶

Back

Close

Full Screen / Esc

Printer-friendly Version

Interactive Discussion

**Table 5.** Number and period(s) of match-up field RLw measurements in each CoastColour site and by Data Provider.

CoastColour site	Data provider	Number	Period
Acadia	NOMAD	76	Apr 2005 to Sep 2007
Benguela	CSIR	84	Mar 2005 to Mar 2008
Cape Verde	NOMAD	8	Oct 2005, Nov 2005
Chesapeake Bay	NOMAD	81	Mar 2005, May 2007
Florida	NOMAD	85	Jan 2005, Oct 2006
Great Barrier Reef	CSIRO	15	Sep 2007, Apr 2008
Gulf of Mexico	MSU(6) NOMAD(41)	47	Dec 2005 May 2007 to Jul 2007
Indonesian waters	ITC(119) NOMAD(8)	127	May 2008, Aug 2009 Apr 2007
Morocco-W. Md. Sea	NOMAD	3	Oct 2005
North Sea	GKSS(48) NOMAD(6)	54	Apr 2005 to Jul 2006 Oct 2005
Oregon-Washington	CEOAS	47	May 2009 to Jul 2010
Southern California	UCSB(303) NOMAD(16)	319	Jan 2005 to Mar 2010 May 2006 to Aug 2007
Trinidad and Tobago	NOMAD	11	Jan 2006 to Mar 2007
All		957	Jan 2005 to Jul 2010

## CoastColour Round Robin datasets

B. Nechad et al.

Title Page

Abstract

Instruments

Data Provenance &amp; Structure

Tables

Figures

◀

▶

◀

▶

Back

Close

Full Screen / Esc

Printer-friendly Version

Interactive Discussion



**Table 6.** Instruments and methods of measurement of RLW in the CCRR match-up dataset.  $\theta_v$  and  $\Delta\varphi$  denote respectively the sensor zenith angle and its azimuth angle relative to the sun. Ed, Lu and Lsky denote respectively the downwelling irradiance, the upwelling radiance and the sky radiance measured along the viewing angle  $\theta_v$ . The indices + and – refer to measurements just above and below the water surface respectively.

Data provider	Instruments	Method	Reference
CEOAS	3 Satlantic HyperPro	Underwater profiling of Lu–, Ed–, and above water Ed+	<a href="http://satlantic.com/sites/default/files/documents/ProSoft-7.7-%20Manual.pdf">http://satlantic.com/sites/default/files/documents/ProSoft-7.7-%20Manual.pdf</a>
CSIR	2 TriOS RAMSES	Floating buoy attached to ship, measuring Lu–, Ed+	N/A
CSIRO	1 TriOS RAMSES	Above water Lu+, Lsky, Ed+. Viewing $\theta_v = 45^\circ$ , $\Delta\varphi \sim 135^\circ$	(Tilstone et al., 2002)
GKSS	3 TriOS RAMSES	Lu+, Lsky, Ed+. Viewing $\theta_v = 45^\circ$ , $\Delta\varphi \sim 135^\circ$	N/A
ITC	2 TriOS RAMSES	Lu+, Lsky, Ed+, $\theta_v = 40^\circ$ , $\Delta\varphi = 135^\circ$	N/A
MSU	N/A	N/A	N/A
NOMAD	Various	In-water profiling, or above-water instruments	(Werdell and Bailey, 2005)
UCSB	N/A	N/A	N/A

[Title Page](#)[Abstract](#)[Instruments](#)[Data Provenance & Structure](#)[Tables](#)[Figures](#)[◀](#)[▶](#)[◀](#)[▶](#)[Back](#)[Close](#)[Full Screen / Esc](#)[Printer-friendly Version](#)[Interactive Discussion](#)**Table 7.** The navigation, L2R and L2W parameters, atmospheric, ancillary and flags products as provided in the MERIS match-up dataset, as 5 × 5 box around the locations of the match-up field measurements. The “critical” flags listed in italic fonts are associated to pixels being rejected (if the flags are raised) in the post-processed MERIS match-up dataset.

Navigation	Description	Units	L2R, L2W	Description	Units
ProdID		–	reflec_x	RLw at $\lambda$ (nm)	–
CoordID	id of location	–	b_tsm	Scattering coefficient at 443 nm	m <sup>-1</sup>
Name	Match-up name	–	a_tot	Total absorption coefficient (443 nm)	m <sup>-1</sup>
Latitude, Longitude	Geographical coordinates	degree			
			Atmosphere	Description	Units
Date, Time			tau_nnn	Aerosol optical thickness at nnn (nm)	–
lat_corr, lon_corr	Ortho-corrected latitude/longitude	degree	ang_443_865	Aerosol Angström coefficient between 443 and 865 nm	–
dem_alt	DEM <sup>1</sup> model altitude	–			
dem_rough	Roughness at sight with intersection of line of WGS84 <sup>2</sup> ellipsoid taken from DEM	degree	Ancillary	Description	Units
sun_view_zenith	Sun, view zenith angle	degree	zonal_wind	ECMWF <sup>3</sup> zonal wind	m s <sup>-1</sup>
sun_view_azimuth	Sun, view azimuth angle	degree	merid_wind	ECMWF meridional wind	m s <sup>-1</sup>
pins	–	–	glint_ratio	Glint ratio	–
ground_control_points	–	–	atm_press	ECMWF atmospheric pressure at mean sea level	hPa
detector_index	Index of MERIS pixel	–	ozone	ECMWF ozone concentration	DU
			rel_hum	ECMWF relative humidity at 850 hPa	%
Flags	Description		Flags	Description	
<i>land</i>	Land pixel		coastline	Pixel is part of a coastline	
<i>water</i>	Water pixel		cosmetic	Cosmetic flag	
<i>cloud_ice</i>	Very high <i>Rtoa</i> indicating cloud, ice or snow pixel		duplicated	Pixel has been duplicated (filled in)	
bright	Bright pixel		f_meglint	Pixel corrected for glint	
<i>sun_glint</i>	Pixel affected by sun glint		f_oinld	Low inland water flag	
glint_risk	Glint correction not reliable on the pixel		f_island	Island flag	
<i>suspect</i>	Suspect flag (from L1 <sup>4</sup> )		f_landcons	Land product available	
<i>invalid</i>	Pixel is invalid		f_ice	Ice pixel	
solzen	High sun zenith angle		f_cloud	IDEPIX <sup>5</sup> final cloud flag	
ancil	Unreasonable data for ozone or pressure		f_bright	IDEPIX bright pixel	
has_flint	If the atmospheric correction used the Flint processor		f_bright_rc	IDEPIX old bright pixel	
l1_flags	Level 1 classification and quality flag		f_low_p_pscatt	IDEPIX test on apparent scattering	
l1p_flags	Pixel classification flag (e.g. cloud screening, land, water)		f_low_p_p1	IDEPIX test on P1	
atc_oor	If RLw is out of the expected range (as set in the NN <sup>5</sup> )		f_slope_1	IDEPIX spectral slope test 1 flag	
toa_oor	Input <i>Rtoa</i> is out of the NN training range		f_slope_2	IDEPIX spectral slope test 2 flag	
tosa_oor	Input <i>Rtosa</i> is out of the NN training range		f_bright_toa	IDEPIX second bright pixel test	
			f_high_mdsi	IDEPIX MDSI <sup>7</sup> above threshold	
			f_snow_ice	IDEPIX snow/ice flag	
			agc_flags	Flag specific to the atmospheric and flint correction	
			agc_land	Land pixel	
			agc_invalid	Pixel not considered for processing	

<sup>1</sup> DEM designates the Digital Elevation Model of altitude. <sup>2</sup> WGS84 refers to the World Geodetic Standard 1984.<sup>3</sup> ECMWF is the European Centre for Medium range Weather Forecast. <sup>4</sup> L1 is MERIS Level 1 product. <sup>5</sup> NN is the atmosphere Neural Network algorithm. <sup>6</sup> IDEPIX is a generic pixel classification algorithm for optical Earth observation sensors. <sup>7</sup> MDSI is the MERIS Differential Snow Index.

CoastColour Round  
Robin datasets

B. Nechad et al.

Title Page

Abstract

Instruments

Data Provenance &amp; Structure

Tables

Figures

◀

▶

◀

▶

Back

Close

Full Screen / Esc

Printer-friendly Version

Interactive Discussion



**Table 8.** The  $5 \times 5$  box averaged L2R, L2W and atmospheric parameters derived from the MERIS match-up dataset.

Navigation	Description	Units	L2R, L2W	Description	Units
Fid	Match-up name	–	RLw_xxx <sup>a</sup>	RLw at $\lambda$ (nm)	–
Latitude, longitude	Geographical coordinates	degrees	b_tsm <sup>a</sup>	Scattering coefficient at 443 nm,	$m^{-1}$
Date, time			a_tot <sup>a</sup>	Total absorption coefficient (443 nm)	$m^{-1}$
sun_view_zenith	Sun, view zenith angle	degrees	Atmosphere	Description	Units
sun_view_azimuth	Sun, view azimuth angle	degrees	tau_nnn <sup>a</sup>	Aerosol optical thickness at nnn (nm)	–
			ang_443_865 <sup>a</sup>	Aerosol Angström coefficient between 443 and 865 nm	–
Box-averaging information	Description	Units	Ancillary	Description	Units
$N(\text{var}^b)$	Number of pixels within the $5 \times 5$ box where valid var was retrieved	–	zonal_wind	ECMWF <sup>c</sup> zonal wind	$ms^{-1}$
			merid_wind	ECMWF meridional wind	$ms^{-1}$
			glint_ratio	Glint ratio	–
std(var <sup>b</sup> )	Standard deviation of var over the $N$ valid pixels in the $5 \times 5$ match-up box	var unit	atm_press	ECMWF atmospheric pressure at mean sea level	hPa
			ozone	ECMWF ozone concentration	DU
			rel_hum	ECMWF relative humidity at 850 hPa	%

<sup>a</sup> Averaged over  $N$  valid pixels in the  $5 \times 5$  box around the match-up location.

<sup>b</sup> The variable var refers to one of the MERIS L2 products listed under L2R, L2W and Atmosphere datatypes.

<sup>c</sup> ECMWF is the European Centre for Medium range Weather Forecast.



CoastColour Round  
Robin datasets

B. Nechad et al.

Title Page

Abstract

Instruments

Data Provenance &amp; Structure

Tables

Figures



Back

Close

Full Screen / Esc

Printer-friendly Version

Interactive Discussion

**Table 10.** Atmospheric, air–sea interface, solar and viewing geometry specifications in CCRRv1.

Parameter	Values
Sun angles	Zenith: 0°, 40° and 60°, azimuth: 0°
Viewing angles	Zenith: 0°, azimuth: 90°
Surface wind speed	5 ms <sup>-1</sup>
Cloud fraction	0
Sky radiance distribution	Semi-empirical sky model (Harrison and Coombes, 1998)
Direct and diffuse sky irradiances	Semi-empirical sky model RADTRAN

CoastColour Round  
Robin datasets

B. Nechad et al.

Title Page

Abstract

Instruments

Data Provenance &amp; Structure

Tables

Figures

I◀

▶I

◀

▶

Back

Close

Full Screen / Esc

Printer-friendly Version

Interactive Discussion

**Table 11.** The inherent optical properties as established in the CCRRv1.

Parameter and value	Description	Reference
$c_{\text{phy}}(660 \text{ nm}) = 0.407 \text{ CHL}^{0.795}$ $Y_{\text{CHL} > 2} = 0$ $Y_{\text{CHL} \leq 2} = 0.5 \log_{10}(\text{CHL}) - 0.3$	Phytoplankton beam attenuation coefficient at 660 nm Spectral variation of $c_{\text{phy}}$ (power law exponent)	Loisel and Morel (1998) Morel et al. (2002)
$\beta_{\text{phy}}(\lambda)$ : FournierForand	Phytoplankton scattering phase function with $b_{\text{bphy}}/b_{\text{phy}} = 0.006$	Similar to Morel et al. (2002)
$a_{\text{p}}^*(\lambda) = A(\lambda) \text{CHL}^{B(\lambda)}$	Phytoplankton specific absorption coefficient	Bricaud et al. (1998)
$b_{\text{MP}}^*(555 \text{ nm}) = 0.51 \text{ m}^2 \text{ g}^{-1}$	Specific scattering coefficient for MP	Babin et al. (2003a)
$\beta_{\text{MP}}(\lambda)$ : Petzold	MP scattering phase function	Mobley (1994)
$a_{\text{MP}}^*(443 \text{ nm}) = 0.04 \text{ m}^2 \text{ g}^{-1}$	Specific absorption coefficient for MP	Babin et al. (2003b)
$S_{\text{MP}} = -0.0123 \text{ nm}^{-1}$	Spectral slope of $a_{\text{MP}}^*$ (exponential)	Babin et al. (2003b)
$Y_{c_{\text{MP}}} = -0.3749$	Spectral variation of the beam attenuation coefficient for MP (power law), giving $b_{\text{p}}^{715}/b_{\text{p}}^{555} = 0.925$	In agreement with Babin et al. (2003a)
$S_{\text{CDOM}} = -0.0176 \text{ nm}^{-1}$	Spectral slope of $a_{\text{g}}$ (exponential)	Babin et al. (2003b)

CoastColour Round  
Robin datasets

B. Nechad et al.

Title Page

Abstract

Instruments

Data Provenance &amp; Structure

Tables

Figures

◀

▶

◀

▶

Back

Close

Full Screen / Esc

Printer-friendly Version

Interactive Discussion

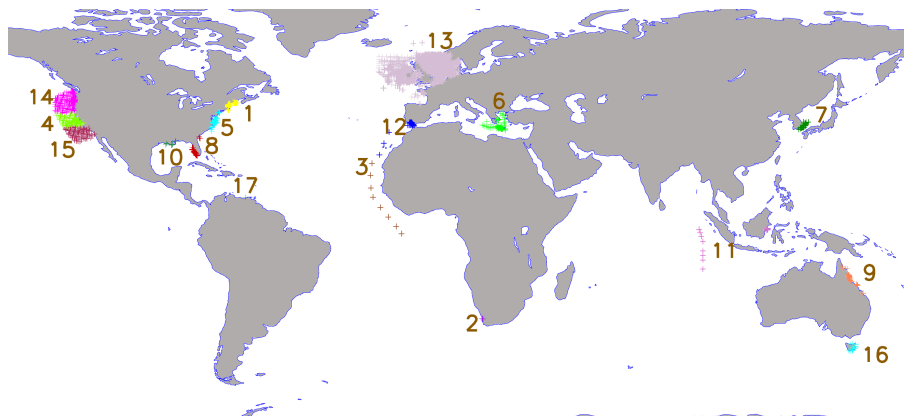


**Figure 1.** The distribution of the in situ data within the 17 CoastColour sites which are, numbered alphabetically, the coastal waters off: (1) Acadia; (2) Benguela; (3) Cape Verde; (4) Central California; (5) Chesapeake Bay; (6) the Eastern Mediterranean Sea (referred to hereafter by E. Md. Sea); (7) the East China Sea; (8) Florida; (9) the Great Barrier Reef region (hereafter GBR region); (10) Gulf of Mexico; (11) Indonesia ; (12) Morocco and western Mediterranean Sea (hereafter Morocco-W. Md. Sea); (13) the North Sea region extending to the English Channel, the Celtic and Irish Seas, the Bay of Biscay and Southern Brittany (all referred to as the North Sea); (14) Oregon-Washington; (15) Southern California; (16) Tasmania; and (17) Trinidad and Tobago.

CoastColour Round  
Robin datasets

B. Nechad et al.

Title Page

Abstract

Instruments

Data Provenance &amp; Structure

Tables

Figures



Back

Close

Full Screen / Esc

Printer-friendly Version

Interactive Discussion

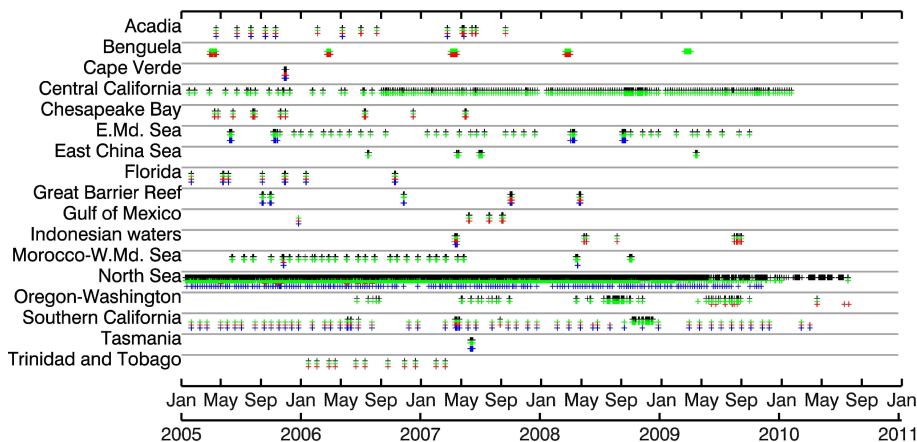


**Figure 2.** Time availability of at least one parameter available from the CoastColour sites within the match-up field measurements: metadata (black) (excluding the date, time and geographical coordinates and the data provider), biogeochemical data (green), AOPs (red) and IOPs (blue).

## CoastColour Round Robin datasets

B. Nechad et al.

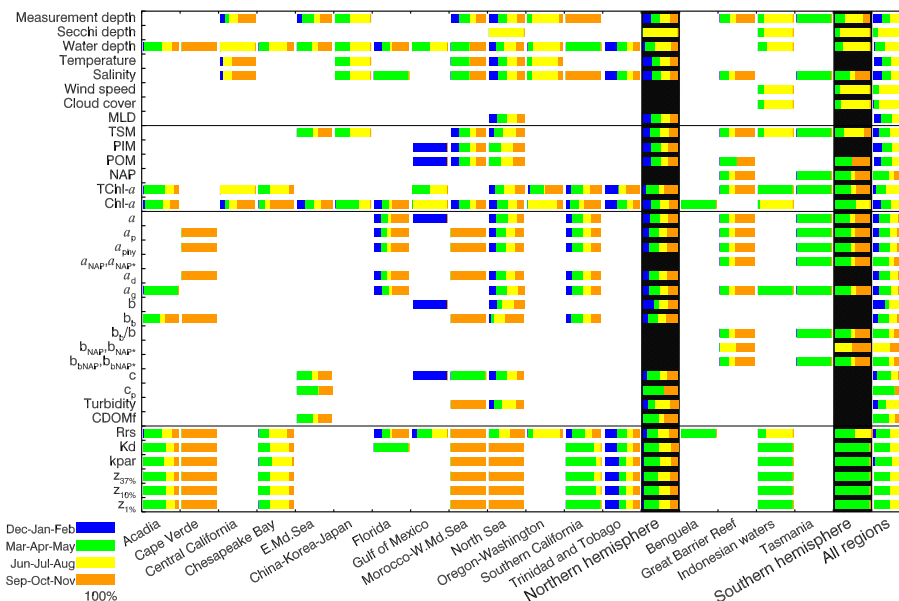


**Figure 3.** Seasonal availability of the metadata, biogeochemical, IOP and AOP measurements from the CoastColour sites within the CCRR match-up dataset.

Title Page

Abstract Instruments

Data Provenance & Structure

Tables Figures

◀ ▶

◀ ▶

Back Close

Full Screen / Esc

Printer-friendly Version

Interactive Discussion



## CoastColour Round Robin datasets

B. Nechad et al.

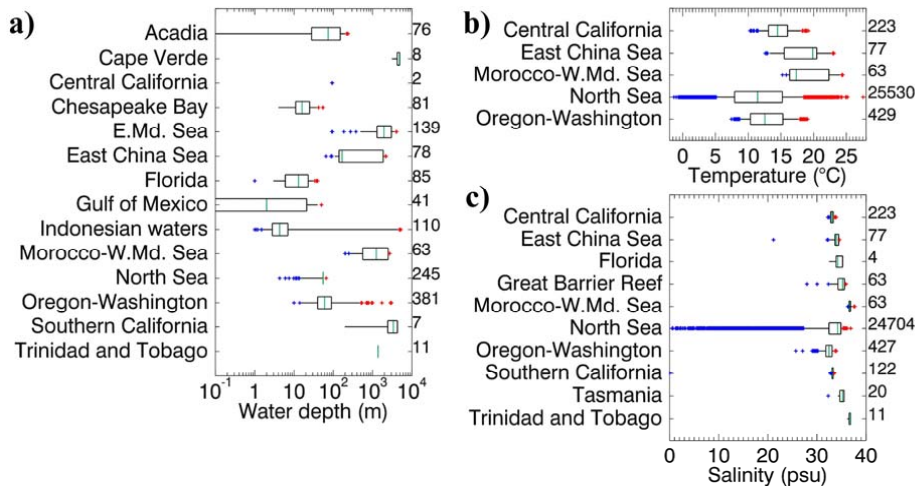


**Figure 4.** MERIS CoastColour processing.

Title Page

Abstract Instruments

Data Provenance & Structure

Tables Figures

◀ ▶

◀ ▶

Back Close

Full Screen / Esc

Printer-friendly Version

Interactive Discussion



CoastColour Round  
Robin datasets

B. Nechad et al.

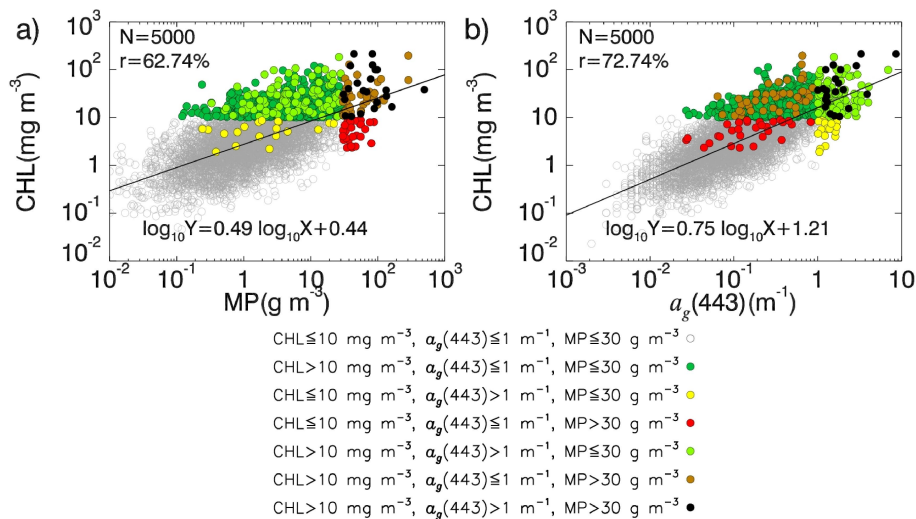


**Figure 5.** The simulated (a) MP and (b)  $a_g(443)$  vs. the simulated CHL concentrations, in the CCRRv1. The colours represent the ranges of MP, CHL and  $a_g(443)$  as reported in the key above.

CoastColour Round Robin datasets

B. Nechad et al.

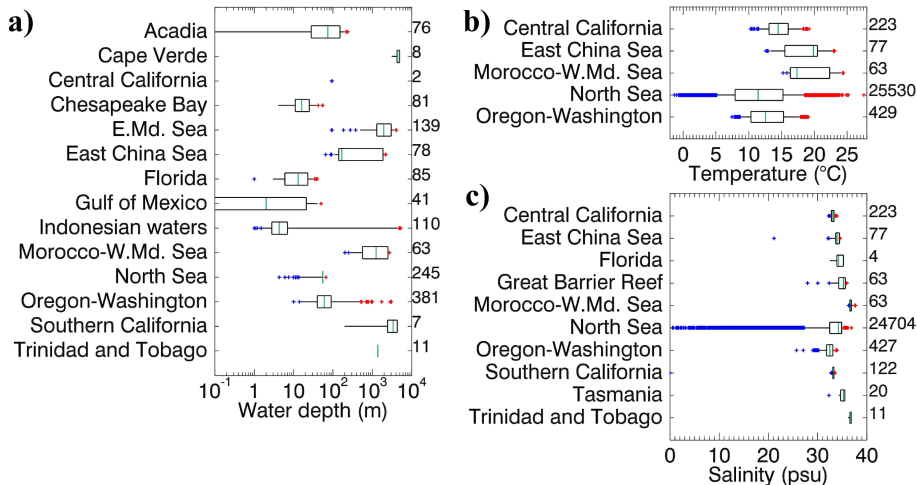


**Figure 6.** The distribution of **(a)** water depth (m); **(b)** temperature (°C); and **(c)** salinity (psu) as given in the in situ dataset at all available depths. The black boxes delimit the percentiles 0.25 and 0.75 of the data and the black horizontal lines show the extension of up to percentiles 0.05 and 0.95. The green line represents the median value and the blue (and red) “+” the minimum (and maximum) plot values below (and above) the percentile 0.05 (0.95). The number of measurements taken at each test site is reported on the right axis of the graph. The scale is logarithmic for the water depth.

Title Page

Abstract Instruments

Data Provenance & Structure

Tables Figures

◀ ▶

◀ ▶

Back Close

Full Screen / Esc

Printer-friendly Version

Interactive Discussion



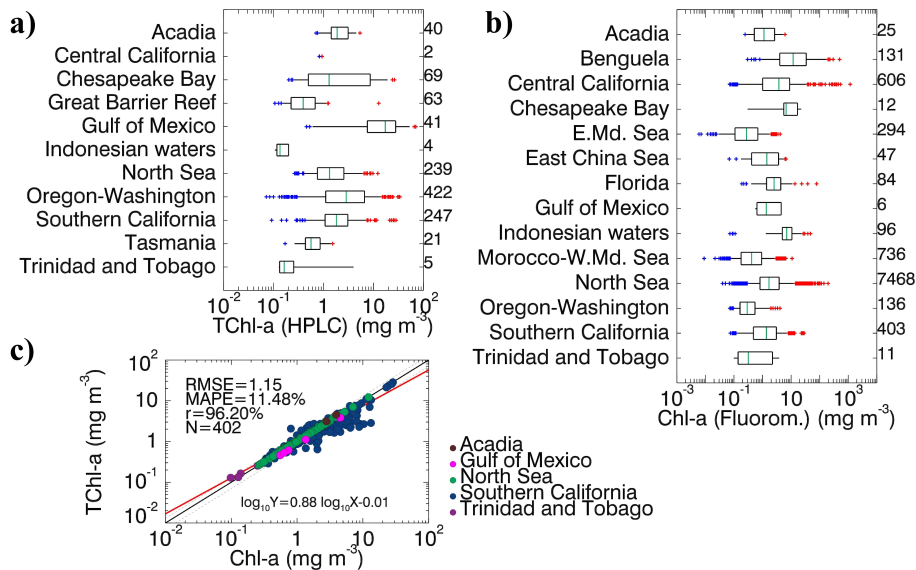


**Figure 7.** The distribution of **(a)** TChl *a* and **(b)** Chl *a* concentrations (in  $\text{mg m}^{-3}$ ) as given in the in situ dataset at all measurement depths, and **(c)** Chl *a* vs. TChl *a*. The number of measurements taken at each test site is reported on the right axis of the graph. The graphical convention in **(a and b)** is identical to Fig. 6. In **(c)** the solid line represents the 1 : 1 ratio and the dashed lines  $\pm 30\%$ .

Title Page

Abstract Instruments

Data Provenance & Structure

Tables Figures

◀ ▶

◀ ▶

Back Close

Full Screen / Esc

Printer-friendly Version

Interactive Discussion



CoastColour Round  
Robin datasets

B. Nechad et al.

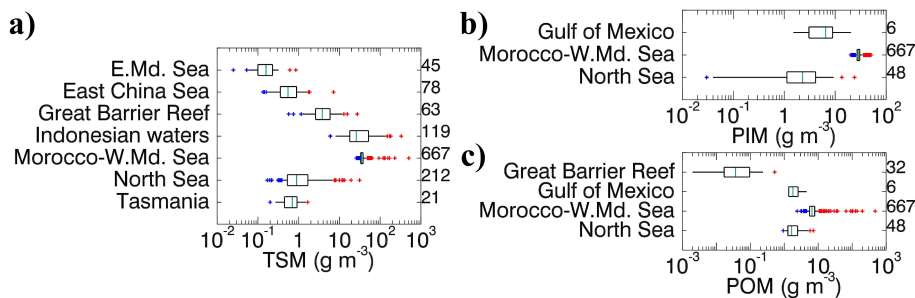


**Figure 8.** The distribution of **(a)** TSM ( $\text{g m}^{-3}$ ), **(b)** PIM ( $\text{g m}^{-3}$ ) and **(c)** POM ( $\text{g m}^{-3}$ ) as given in the in situ dataset at all measurement depths. The number of measurements taken at each test site is reported on the right axis of the graphs. The graphical convention is identical to Fig. 6.

Title Page

Abstract

Instruments

Data Provenance &amp; Structure

Tables

Figures

◀

▶

◀

▶

Back

Close

Full Screen / Esc

Printer-friendly Version

Interactive Discussion



CoastColour Round Robin datasets

B. Nechad et al.

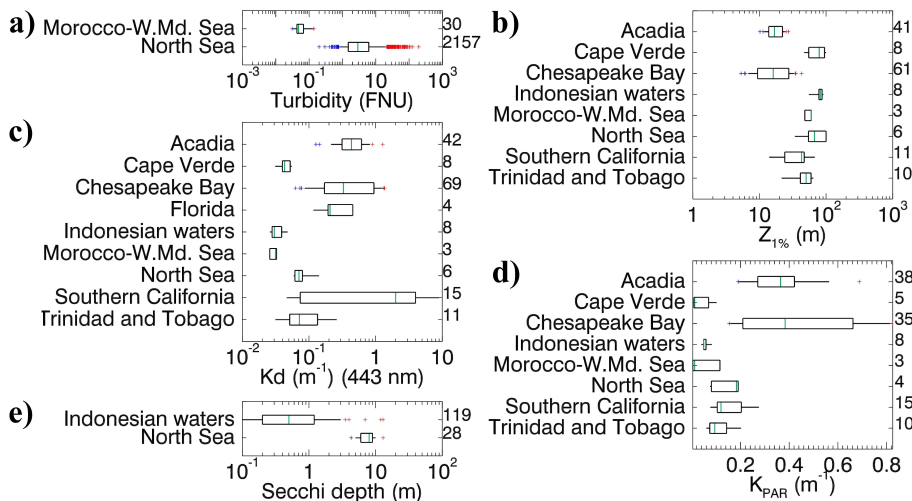


**Figure 9.** The distribution of **(a)** turbidity (FNU for the North Sea and FTU for Morocco-W. Md. Sea), **(b)** the photic depth  $Z_{1\%}$  (m), **(c)**  $K_d$  at 443 nm ( $m^{-1}$ ), **(d)**  $K_{PAR}$  ( $m^{-1}$ ) and **(e)** Secchi depth (m). The scale is logarithmic for turbidity and  $K_d$ , and linear elsewhere. The number of measurements taken at each test site is reported on the right axis of the graph. The graphical convention is identical to Fig. 6.

Title Page

Abstract Instruments

Data Provenance & Structure

Tables Figures

◀ ▶

◀ ▶

Back Close

Full Screen / Esc

Printer-friendly Version

Interactive Discussion



CoastColour Round Robin datasets

B. Nechad et al.

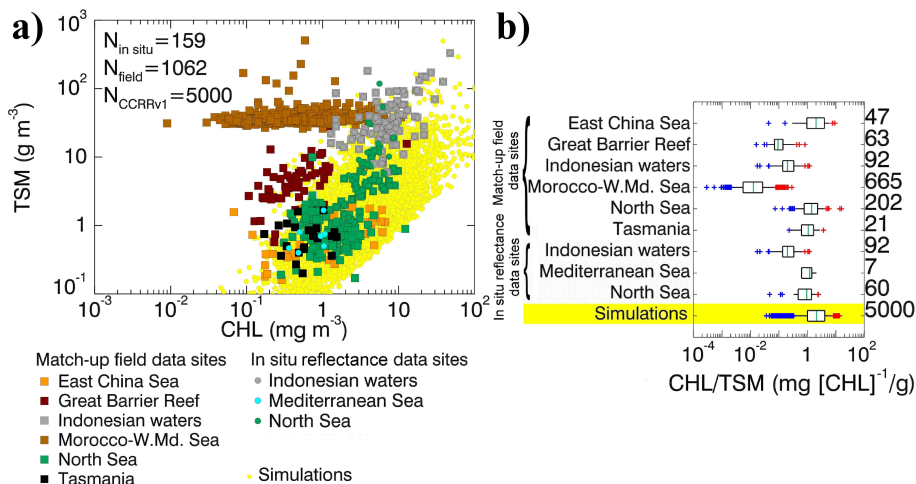


**Figure 10.** The distribution of **(a)** CHL concentrations ( $\text{mg m}^{-3}$ ) vs. TSM concentrations ( $\text{g m}^{-3}$ ) from the in situ reflectance dataset (in the three sites as indicated in the key) plotted as filled circles, and from the match-up dataset, including Chl *a* and TChl *a* (where available), and the associated match-up field TSM concentrations (in the six sites indicated in the key) and plotted as filled squares, both superimposed to the simulated data (yellow circles); **(b)** CHL/TSM ratio ( $\text{mg [CHL]}^{-1} \text{g}^{-1}$ ) from the match-up, in situ reflectance and simulated datasets. The graphical convention in **(b)** is identical to Fig. 6, the yellow colour distinguishes the simulated dataset from the in situ measurements.

Title Page

Abstract Instruments

Data Provenance & Structure

Tables Figures

Navigation: Previous, Next, Home, Back, Close

Full Screen / Esc

Printer-friendly Version

Interactive Discussion



CoastColour Round  
Robin datasets

B. Nechad et al.

Title Page

Abstract

Instruments

Data Provenance &amp; Structure

Tables

Figures

◀

▶

◀

▶

Back

Close

Full Screen / Esc

Printer-friendly Version

Interactive Discussion

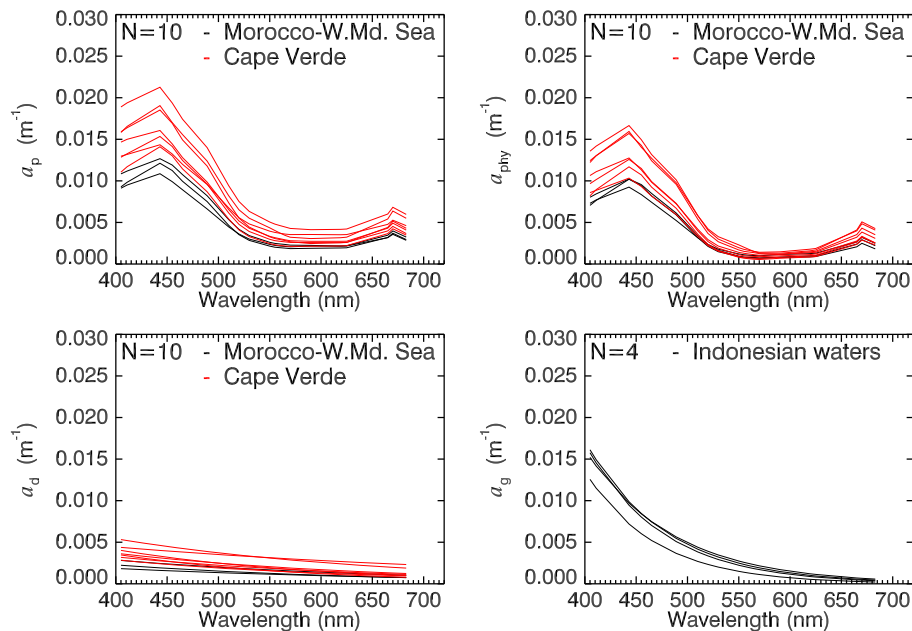


**Figure 11.** The match-up field absorption spectra provided from Morocco-W. Md. Sea, Cape Verde and Indonesian waters.

CoastColour Round  
Robin datasets

B. Nechad et al.

Title Page

Abstract

Instruments

Data Provenance &amp; Structure

Tables

Figures

◀

▶

◀

▶

Back

Close

Full Screen / Esc

Printer-friendly Version

Interactive Discussion

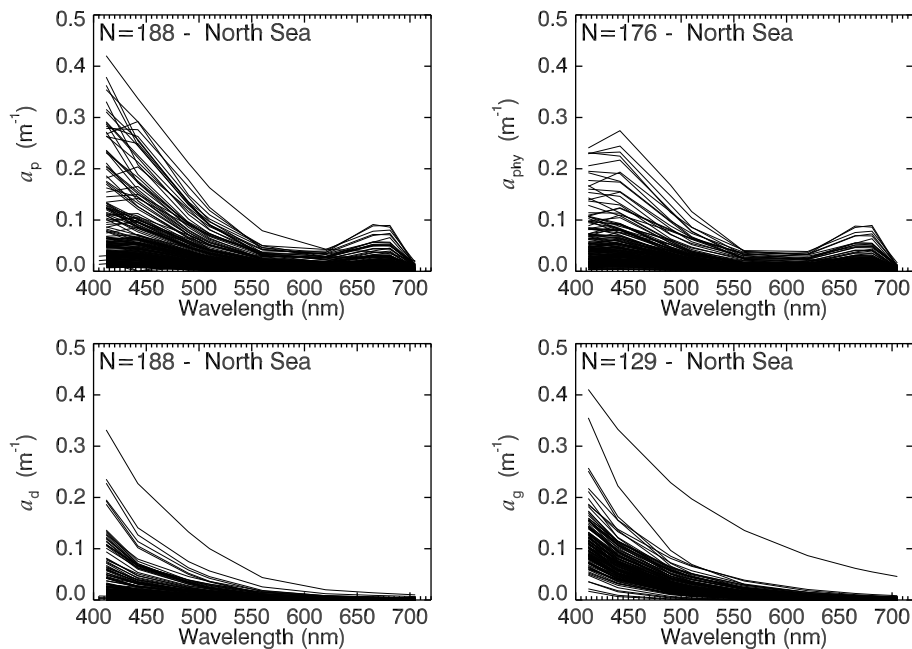


**Figure 12.** The match-up field absorption spectra provided from the North Sea site.

CoastColour Round  
Robin datasets

B. Nechad et al.

Title Page

Abstract

Instruments

Data Provenance &amp; Structure

Tables

Figures

◀

▶

◀

▶

Back

Close

Full Screen / Esc

Printer-friendly Version

Interactive Discussion

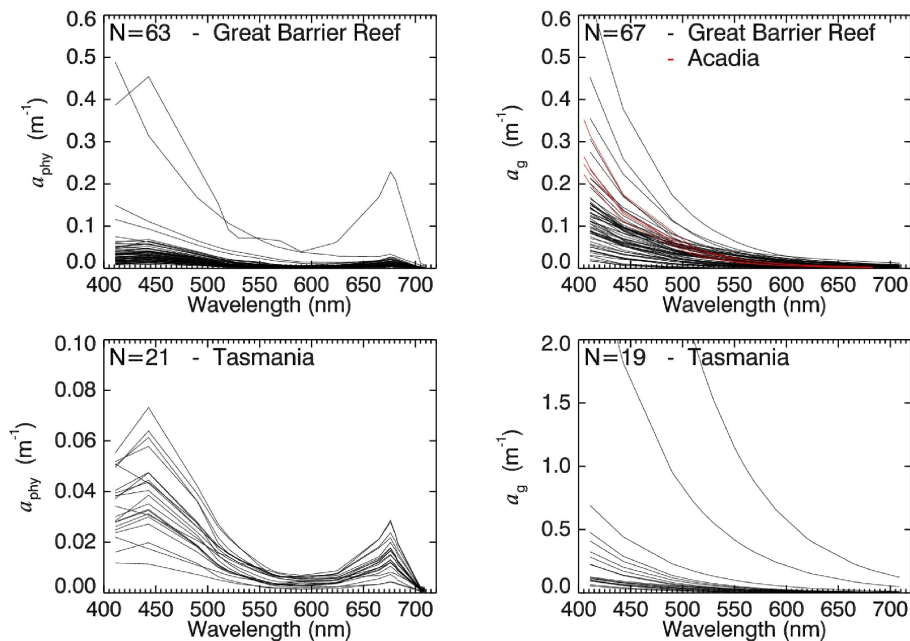


**Figure 13.** The match-up field absorption spectra provided from the GBR region and Acadia (upper panel) and Tasmania (bottom) sites.

CoastColour Round  
Robin datasets

B. Nechad et al.

Title Page

Abstract

Instruments

Data Provenance &amp; Structure

Tables

Figures

◀

▶

◀

▶

Back

Close

Full Screen / Esc

Printer-friendly Version

Interactive Discussion

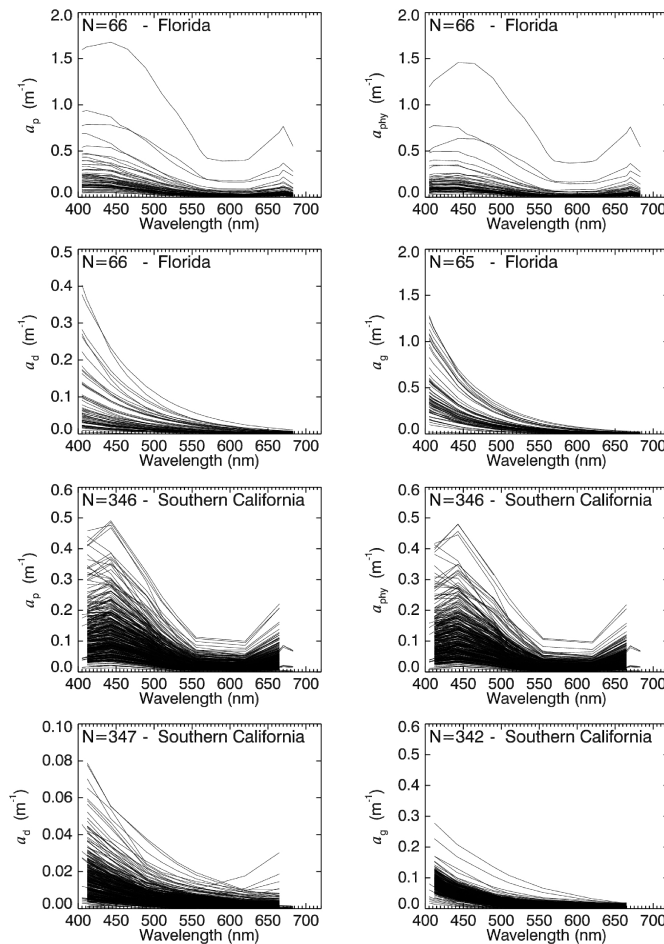


**Figure 14.** The match-up field absorption spectra provided from the Florida (upper panel) and Southern California (bottom) sites.

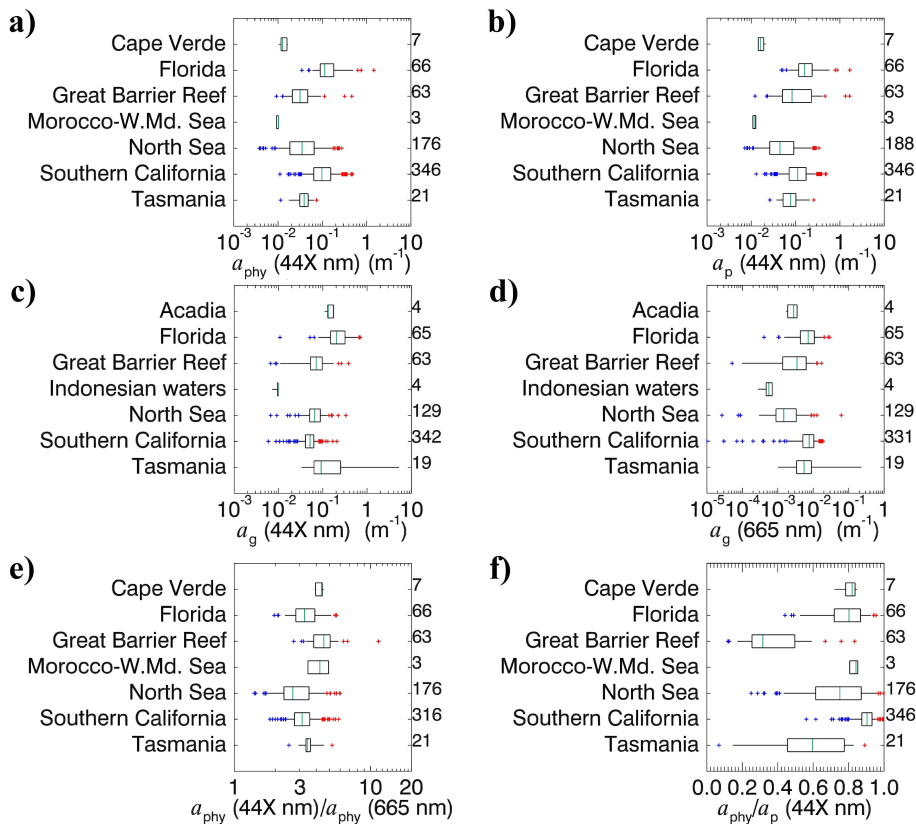


**Figure 15.** The distributions of **(a)**  $a_{\text{phy}}(44\text{X})$ ; **(b)**  $a_{\text{p}}(44\text{X})$ ; **(c)**  $a_{\text{g}}(44\text{X})$ ; **(d)**  $a_{\text{g}}(665)$ ; **(e)** the ratios  $a_{\text{phy}}(44\text{X})/a_{\text{phy}}(665)$  and **(f)**  $a_{\text{phy}}/a_{\text{p}}(44\text{X})$  measured at the CoastColour sites. When coefficients at wavelength 443 nm are missing, they are replaced by data at 440 or 442 nm. The graphical convention is identical to Fig. 6.

CoastColour Round  
Robin datasets

B. Nechad et al.

Title Page

Abstract

Instruments

Data Provenance &amp; Structure

Tables

Figures

◀

▶

◀

▶

Back

Close

Full Screen / Esc

Printer-friendly Version

Interactive Discussion

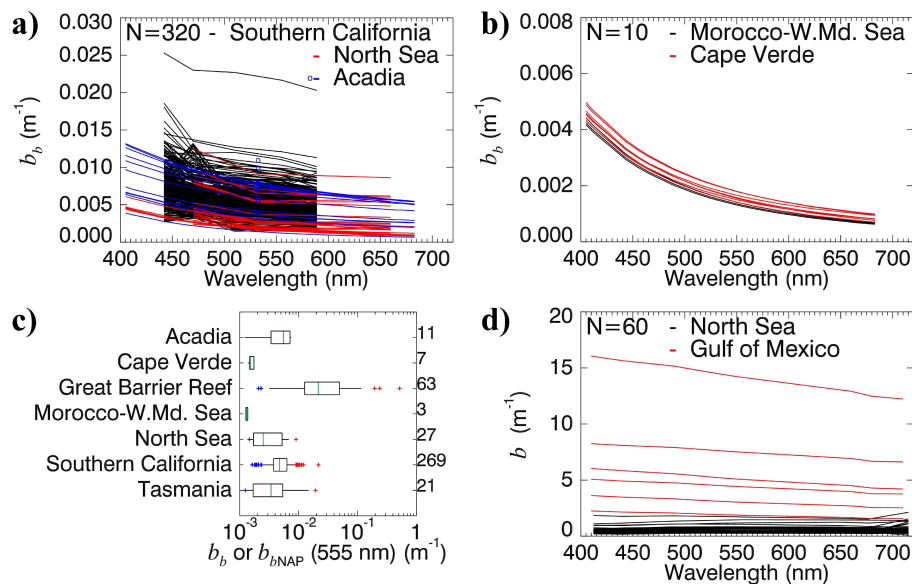


**Figure 16.** The spectra of **(a)**  $b$  ( $\text{m}^{-1}$ ) measured in the Gulf of Mexico and North Sea sites and **(b)**  $b_b$  ( $\text{m}^{-1}$ ) measured in 5 CoastColour sites (note that the coefficients from the Southern California were limited to the spectral range 442–589 nm).

CoastColour Round  
Robin datasets

B. Nechad et al.

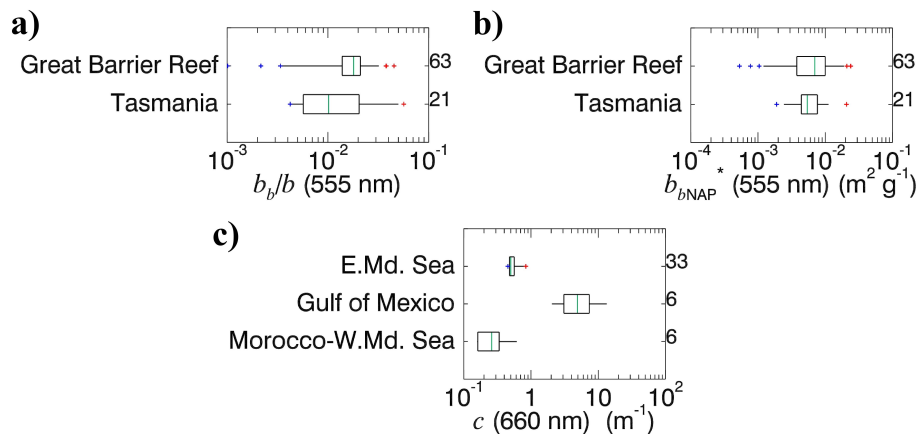


**Figure 17.** The distributions of **(a)**  $b_b/b$  **(b)**  $b_{bNAP}^*$  ( $m^2 g^{-1}$ ) and **(c)**  $c(660)$  ( $m^{-1}$ ). Note the different scaling used for these plots. The graphical convention in Fig. 6 is used.

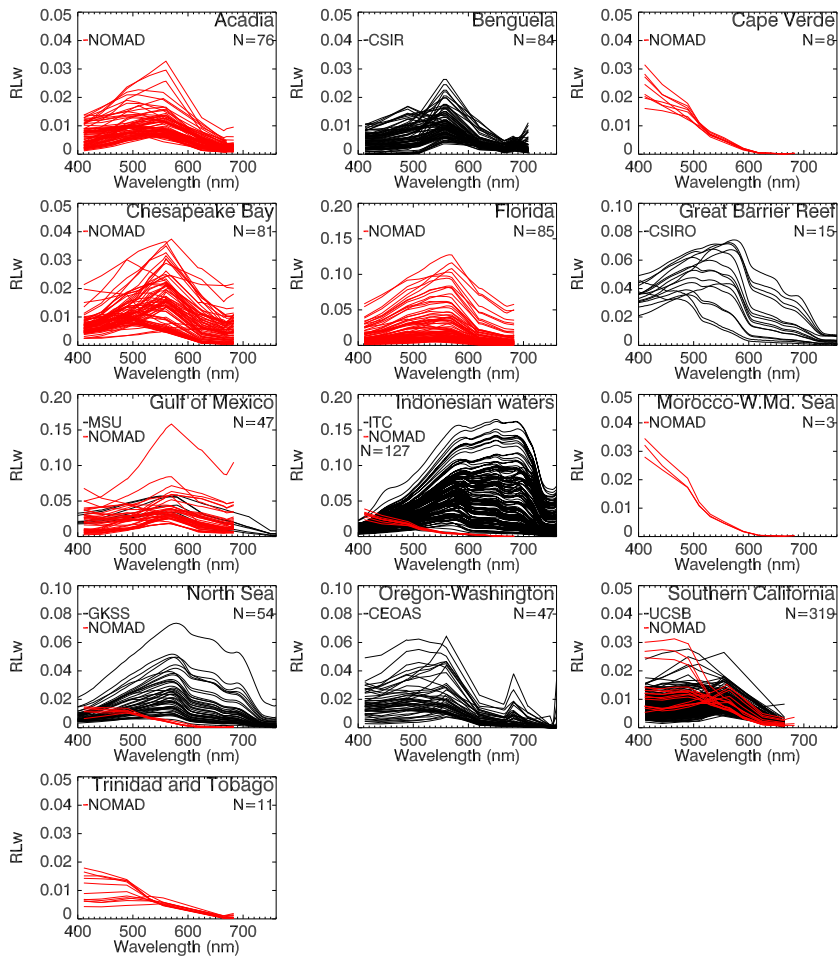


**Figure 18.** Match-up field RLW provided from nine CoastColour sites by the eight Data Providers indicated in the figures. Note the different scales used for the sites.

CoastColour Round  
Robin datasets

B. Nechad et al.

Title Page

Abstract

Instruments

Data Provenance &amp; Structure

Tables

Figures

◀

▶

◀

▶

Back

Close

Full Screen / Esc

Printer-friendly Version

Interactive Discussion

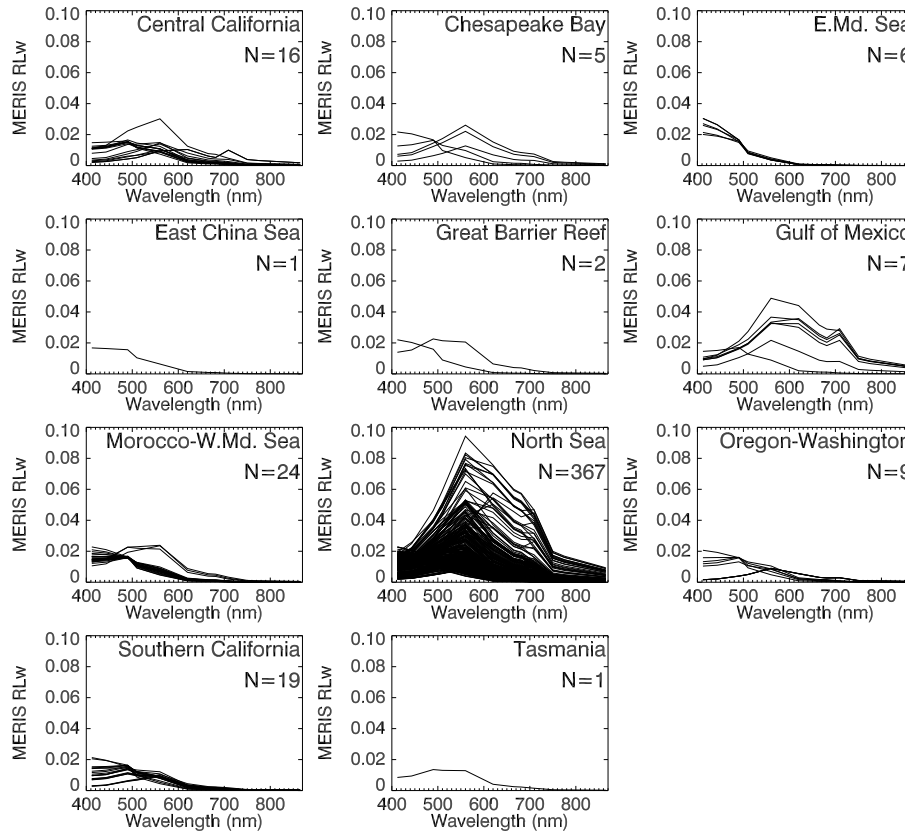
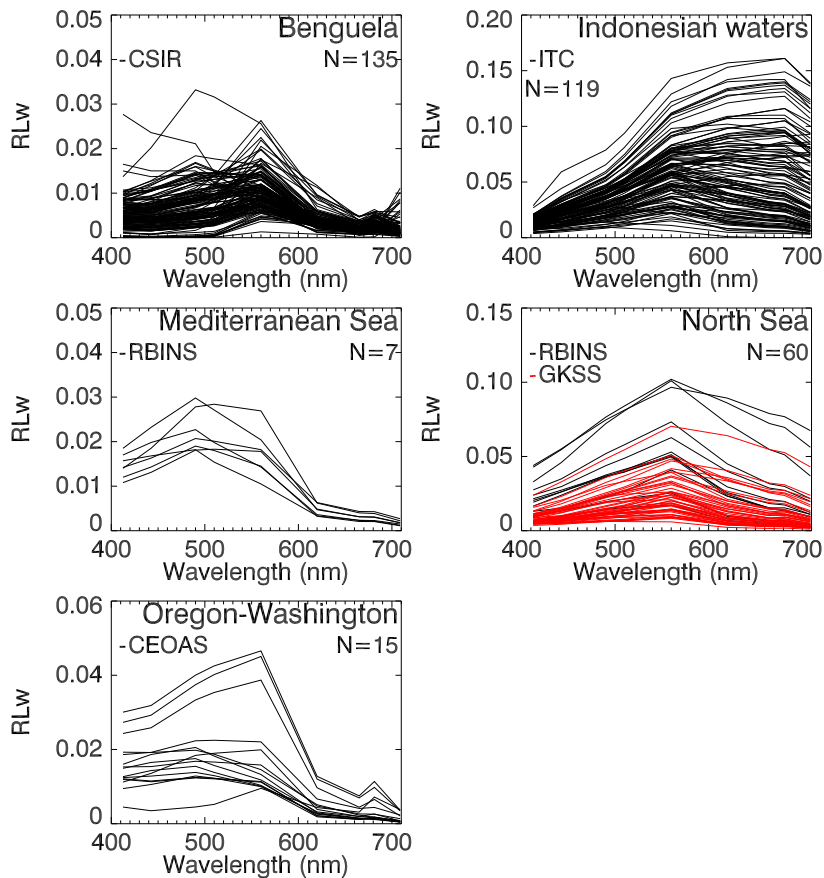


Figure 19. MERIS RLW provided in the CCRR match-up dataset for the 11 CoastColour sites.



**Figure 20.** The in situ reflectance spectra provided from five CoastColour sites. Note the different scales used for the sites. The spectra from the North Sea site coloured in red were provided by GKSS.

CoastColour Round  
Robin datasets

B. Nechad et al.

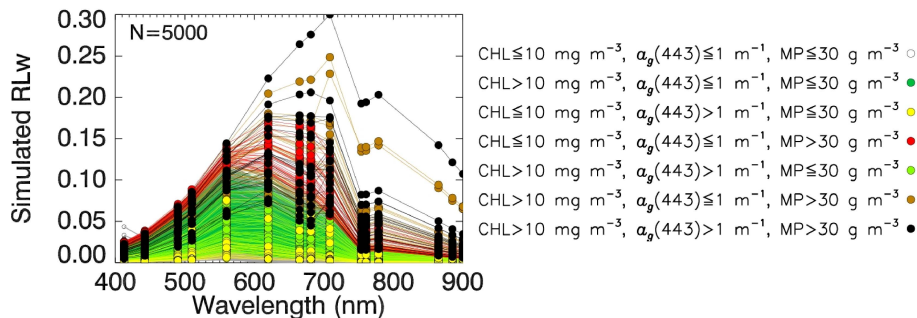


**Figure 21.** The simulated reflectance spectra in the CCRRv1. The colours represent the ranges of MP, CHL and  $a_g(443)$  as reported in the key above.

Title Page

Abstract

Instruments

Data Provenance &amp; Structure

Tables

Figures

◀

▶

◀

▶

Back

Close

Full Screen / Esc

Printer-friendly Version

Interactive Discussion



CoastColour Round  
Robin datasets

B. Nechad et al.

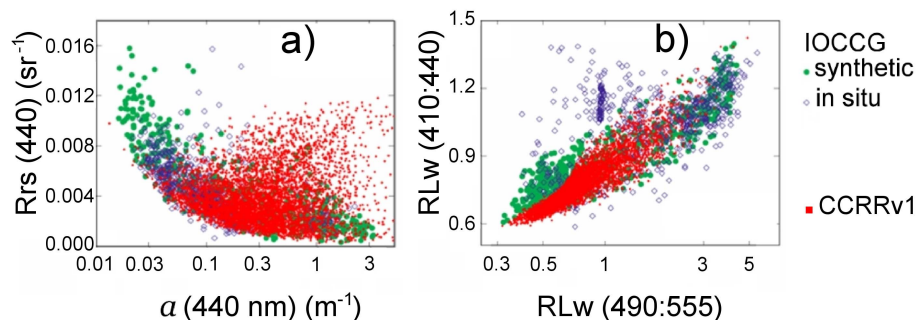


**Figure 22.** Comparison between IOCCG (green), reproduced from Fig. 2.3 in IOCCG (2006) and CCRRv1 (red) simulated datasets. **(a)** variations of the remote sensing reflectance  $R_{rs}(440)$  with  $a(440)$ , **(b)** variations of  $R_{rs}$  band ratio 410 : 440 with respect to  $R_{rs}$  band ratio 490 : 555. The blue diamonds represent the NOMAD (Werdell et al., 2003) subset of in situ data extracted from the SeaBASS dataset and used in the algorithm testing in IOCCG (2006).

## CoastColour Round Robin datasets

B. Nechad et al.

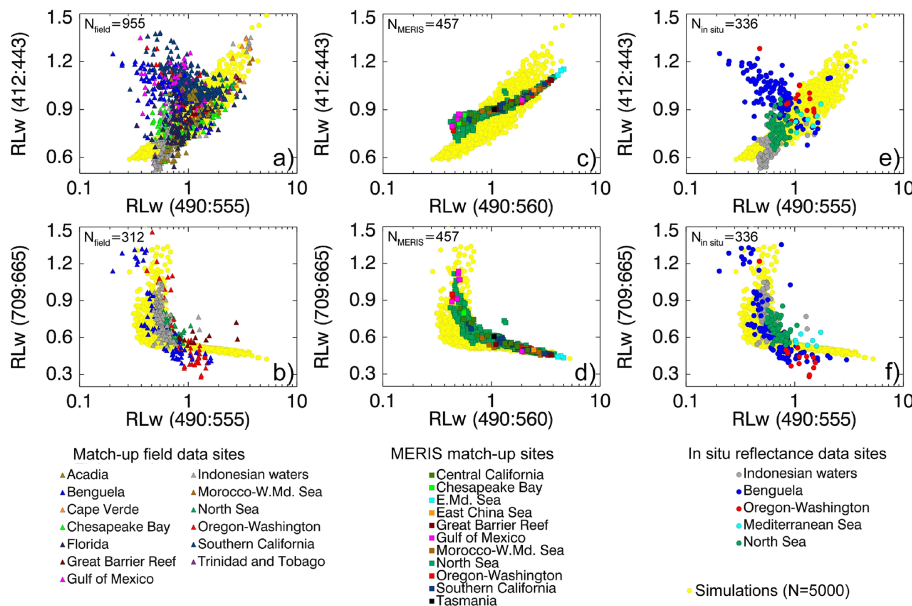


**Figure 23.** RLw band ratio 490 : 555 vs. RLw band ratio 412 : 443 (a) and vs. RLw band ratio 709 : 665 (b) within the match-up field dataset, RLw band ratio 490 : 560 vs. RLw band ratio 412 : 443 (c) and vs. RLw band ratio 709 : 665 (d) within the MERIS RLw products of the match-up dataset, and in the in situ reflectance dataset (e, f). The yellow circles represent the simulated dataset.

Title Page

Abstract Instruments

Data Provenance & Structure

Tables Figures

◀ ▶

◀ ▶

Back Close

Full Screen / Esc

Printer-friendly Version

Interactive Discussion



CoastColour Round  
Robin datasets

B. Nechad et al.

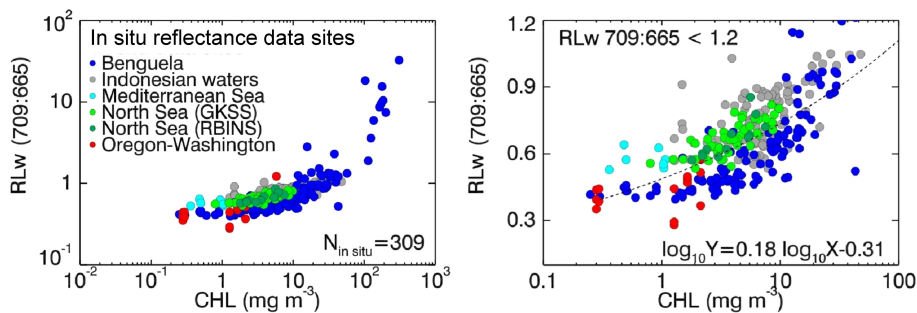


**Figure 24.** From the CCRR in situ reflectance dataset: CHL (mg m<sup>-3</sup>) vs. RLW band ratio 709 : 665 with a zoom on the lower range of RLW 709 : 665 < 1.2 presented in the left figure.

Title Page

Abstract

Instruments

Data Provenance &amp; Structure

Tables

Figures

◀

▶

◀

▶

Back

Close

Full Screen / Esc

Printer-friendly Version

Interactive Discussion



CoastColour Round  
Robin datasets

B. Nechad et al.

Title Page

Abstract

Instruments

Data Provenance &amp; Structure

Tables

Figures

◀

▶

◀

▶

Back

Close

Full Screen / Esc

Printer-friendly Version

Interactive Discussion

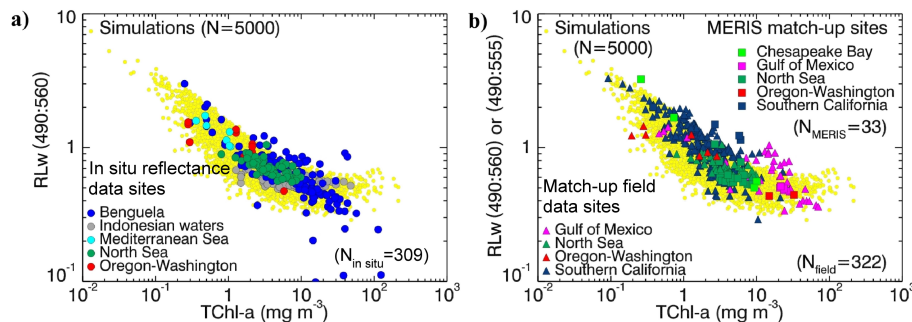


**Figure 25.** Reflectance band ratio 490 : 560 vs. CHL concentrations ( $\text{mg m}^{-3}$ ) from **(a)** the in situ reflectance dataset and from **(b)** MERIS RLw products and match-up field RLw measurements (using band 555 nm instead of 560 nm) with the associated match-up field TChl a concentrations, both superimposed to the simulated reflectance band ratio 490 : 560 vs. the simulated CHL (yellow circles). Match-up field TChl a data are restricted to measurements collected within 1 h after/before the time of MERIS overpass, and to the maximum measurement depth of 2 m.

CoastColour Round  
Robin datasets

B. Nechad et al.

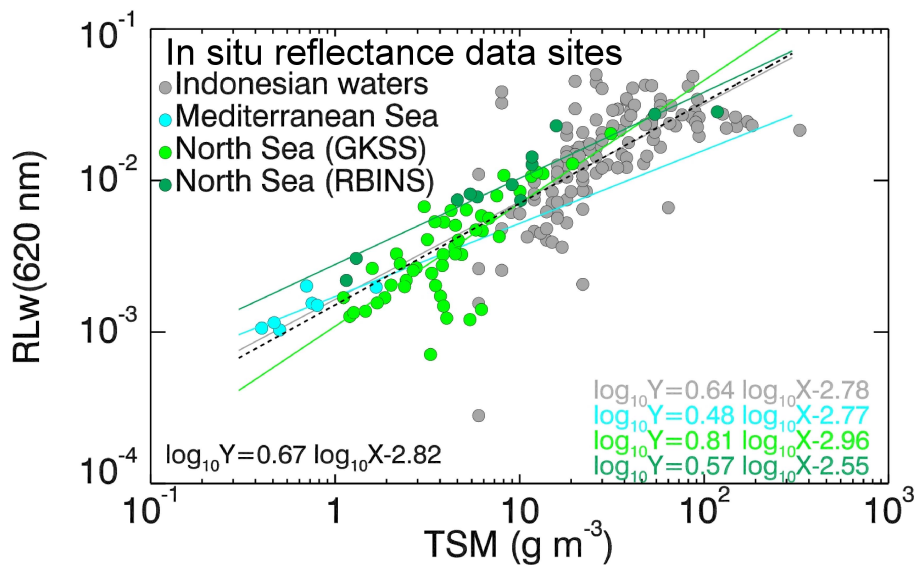


**Figure 26.** TSM ( $\text{g m}^{-3}$ ) vs. RLw(620 nm) from the CCRR in situ reflectance dataset and their associated regression lines.

Title Page

Abstract

Instruments

Data Provenance &amp; Structure

Tables

Figures

◀

▶

◀

▶

Back

Close

Full Screen / Esc

Printer-friendly Version

Interactive Discussion



Title Page

Abstract

Instruments

Data Provenance &amp; Structure

Tables

Figures



Back

Close

Full Screen / Esc

Printer-friendly Version

Interactive Discussion

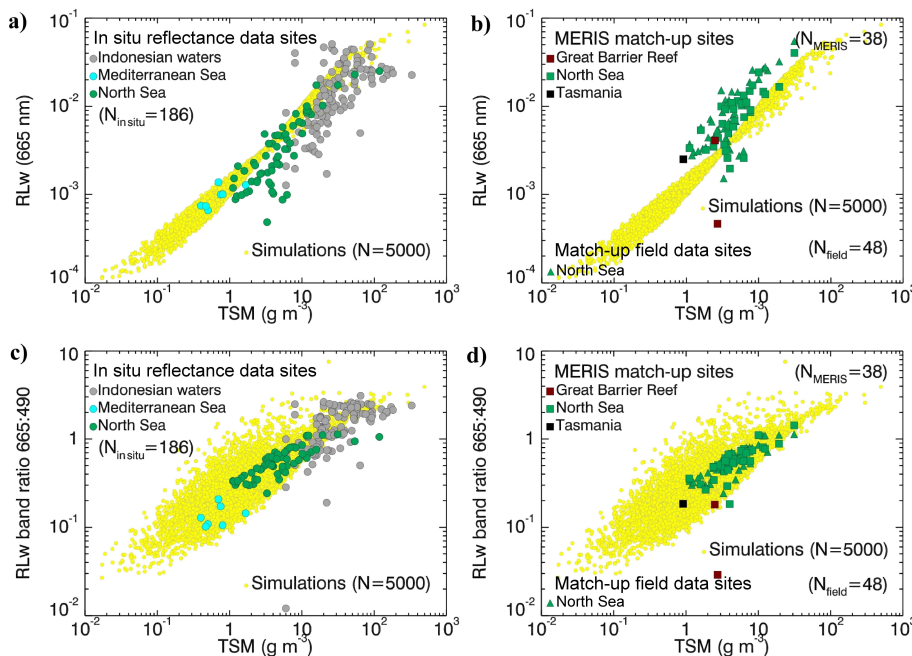


**Figure 27.** The relationships TSM vs. RLW(665) and TSM vs. RLW band ratio 665 : 490 in the in situ reflectance dataset (non-yellow circles) plotted respectively in (a) and (c), in the MERIS and match-up field datasets (squares and triangles) respectively in (b) and (d) and in the simulated dataset (yellow circles) in (a–d).